DENSITY-FUNCTIONAL APPROACHES TO INTERACTING ELECTRONS IN QUANTUM DOTS

Henri Saarikoski

Laboratory of Physics
Helsinki University of Technology
Espoo, Finland

Dissertation for the degree of Doctor of Science in Technology to be presented with due permission of the Department of Engineering Physics and Mathematics for public examination and debate in Auditorium E at Helsinki University of Technology (Espoo, Finland) on the 10th of October, 2003, at 12 o'clock noon.

Dissertations of Laboratory of Physics, Helsinki University of Technology
ISSN 1455-1802

Dissertation 125 (2003):
Henri Saarikoski: Density-functional approaches to interacting electrons in quantum dots
ISBN 951-22-6708-X (print)
ISBN 951-22-6709-8 (electronic)

Otamedia OY
ESPOO 2003

Abstract

Quantum dots are man-made nanoscale structures. As they show typical atomic properties they are often referred to as artificial atoms. The wave functions, shell structure, and energy levels are usually reminiscent of real atomic systems. A wide variety of geometries is possible by choosing appropriate materials and external confinement: one-dimensional rods, two-dimensional pancakes, or three-dimensional spheres. Since quantum dots are nanoscale systems, quantum mechanics is required for their accurate description. However, the electronic structure of these systems is very hard or even impossible to solve exactly even in the case of a few electrons, and approximations must be used.

This thesis concentrates on electronic structure calculations of two-dimensional quantum dot systems, using the density-functional approach. The spin-density-functional theory (SDFT) and the current-spin-density-functional theory (CSDFT) are applied to study the ground-state properties of quantum dot systems in zero and finite magnetic fields. Especially the effects of complex electron-electron interactions are studied.

Emphasis has also been set on developing and testing various methods and approximations. This is done by comparing the ground-state energy and other observables to those obtained using the variational quantum Monte Carlo method. The Kohn-Sham equations of the density-functional theories are solved in real-space by using the Rayleigh quotient multigrid method. This approach is compared to the traditional plane-wave solving methods.

The systems under consideration in this work include single quantum dots with different confining potentials, double quantum dot 'hydrogen' molecule, and a superconductor-normal quantum dot-superconductor (SNS) structure. Symmetry-breaking solutions emerge in these calculations. These include spin-density-wave-like solutions, charge-density-wave-like solutions, Wigner molecule formation, and solutions with vortex structures. The structure and properties of these solutions have been calculated and the interpretation of the broken symmetry is discussed.

Preface

This thesis has been prepared in the Laboratory of Physics at the Helsinki University of Technology during the years 1999–2003. I have been working in the Computational Condensed-Matter and Complex Materials group (COMP).

I wish to express my gratitude to Academy Professor Risto Nieminen for suggesting this research topic to me and providing facilities and conditions for the research. I am indebted to Professor Martti Puska for excellent guidance and supervision during the research work and preparation of the papers. I would also like to thank the members of the Electronic Properties of Materials group for a pleasant research atmosphere. I especially wish to thank M.Sc. Esa Räsänen, Dr. Ari Harju, M.Sc. Sami Siljamäki, and Dr. Tuomas Torsti for contributing to this work, and M.Sc. Klas Engström and Dr. Jari Kinaret in Chalmers University of Technology for fruitful collaboration, Professor Matti Manninen and Dr. Jere Kolehmainen for valuable information and fruitful discussions, and M.Sc. Ivan Degtyarenko for providing and administering excellent computer facilities in the Laboratory. I gratefully acknowledge the financial support of the Kalle Väisälä foundation of the Finnish Academy of Science and Letters which has given me the opportunity to participate in international conferences and present my work there.

Finally I would like to thank Tuuli for proofreading and for her invaluable support during the preparation of this thesis.

Helsinki, May 2003.

Henri Saarikoski

Contents

List of publications

This thesis consists of an overview and the following publications:

I H. Saarikoski, E. Räsänen, S. Siljamäki, A. Harju, M. J. Puska, and R. M. Nieminen, *Electronic properties of model quantum-dot structures in zero and finite magnetic fields*, European Journal of Physics B, **26**, 241–252 (2002) © 2002 EDP Sciences, Società Italiana di Fisica, Springer-Verlag 2002

II H. Saarikoski, M. J. Puska, and R. M. Nieminen, *Electronic structure calculations for two-dimensional quantum dots and laterally coupled quantum-dot molecules in magnetic fields*, International Journal of Quantum Chemistry **91** (3): 490–497 (2003) © 2003 John Wiley & Sons, Inc.

III H. Saarikoski, E. Räsänen, S. Siljamäki, A. Harju, M. J. Puska, and R. M. Nieminen, *Testing of two-dimensional local approximations in the current-spin and spin-density-functional theories*, Physical Review B **67**, 205 327 (2003) © 2003 American Physical Society

IV E. Räsänen, H. Saarikoski, V.N. Stavrou, A. Harju, M. J. Puska, and R. M. Nieminen, *Electronic structure of rectangular quantum dots*, Physical Review B **67**, 235 307 (2003) © 2003 American Physical Society

V E. Räsänen, H. Saarikoski, M. J. Puska, and R. M. Nieminen, *Wigner molecules in polygonal quantum dots: A density-functional study*, Physical Review B, **67**, 035 326 (2003) © 2003 American Physical Society

VI Klas Engström, Jari Kinaret, Robert I. Shekhter, Martti Puska, and Henri Saarikoski, *Influence of electron-electron interactions on current through SNS structures*, Low Temperature Physics (Fizika Nizkikh Temperatur), **29**, 546 (2003) © 2003 American Institute of Physics

VII Klas Engström, Jari Kinaret, Robert I. Shekhter, Henri Saarikoski, and Martti Puska, *Interaction effects in superconductor-normal quantum dot-superconductor structures*, Submitted to Computational Materials Science.

The research presented in this dissertation has been carried out in the Laboratory of Physics in the Computational Condensed-Matter and Complex Materials group (COMP) at the Helsinki University of Technology. The author has had an active role in all the published papers. He has designed the computer programs which have been used to calculate the results in papers I–V and provided program code for the calculations in the preparation of papers VI–VII. The author has written the overview and papers I–III, and contributed to the writing process of papers IV–VII.

Taking Three as the subject to reason about–
A convenient number to state–
We add Seven, and Ten, and then multiply out
By One Thousand diminished by Eight.

The result we proceed to divide, as you see,
By Nine Hundred and Ninety and Two:
Then subtract Seventeen, and the answer must be
Exactly and perfectly true.

Lewis Carroll, The Hunting of the Snark

Chapter 1

INTRODUCTION

Since the advent of the modern microelectronics there has been a constant demand of miniaturization of the electronic circuits towards faster operation speeds and more compact size. This has lead to rapid increase in the computing power and the memory storage capability of the integrated circuits, and to high-performance devices for scientific and industrial applications. The development has triggered a transition from microelectronics towards the nanometer-scale electronics and nanotechnology. The first milestone in this field was the invention of the semiconductor superlattice by Esaki and Tsu in the early 1970's resulting in a new class of transport and optoelectronic devices such as the quantum well lasers. There have been proposals for new device structures and new concepts for the future computers and other electronics devices. For instance, quantum computing could provide a new fruitful approach in supercomputing. New types of nanostructures have been proposed which could provide components for the present day computers as well as for future quantum computers. Especially the quantum dots, man-made nanoscale droplets of electrons trapped in all spatial directions, have many possible technological applications.

The main objective of this work is to study theoretically electronic structures of quantum dot systems by using numerical computations. The physics of such systems is versatile and has received much attention from physicists during recent years. In particular, the complex interplay between interference and interaction effects is a challenging problem and opens new prospects for studying many-body physics both experimentally and theoretically. Results of the theoretical calculations can be compared to experimental data of *e.g.* conductance and scattering measurements. Moreover, results of calculations provide also valuable information of other fermionic systems in different environments.

The reliability and accuracy of the various numerical algorithms and approximations in this field of physics have been subjects of an on-going discussion. Therefore, emphasis has also been set in this work on developing and testing numerical methods. This work adds new data and results which can be used to improve the numerical methods and give qualitative and quantitative conditions when the methods and approximations can provide reliable results.

The organization of the thesis is as follows. Quantum dots and their fabrication methods

will be briefly overviewed in chapter 2. The theoretical basis of this work will be presented in chapter 3. Computational schemes used in the electronic structure calculations are presented in chapters 4 and 5. The spin-density-functional and current-spin-density-functional theories, central in this work, will be presented in detail in chapter 5. The real-space approach used in the numerical calculations will be overviewed in chapter 6. Results of the computations will be presented in chapter 7. And finally the work will be concluded with a summary and discussion in chapter 8. The abstracts of the papers will be found in the appendix.

Chapter 2

QUANTUM DOTS

2.1 Artificial atoms

Quantum dots are small man-made objects which have dimensions of the order of $10^{-8} - 10^{-6}$ m. They can be manufactured from semiconductor materials using modern crystal growth techniques [1–3]. They contain a small controllable number of electrons, usually from 1 to 1000. The droplet of charge is trapped in all spatial dimensions. Depending on the geometry and fabrication techniques, the droplet can be a three-dimensional sphere, a two-dimensional disc, or a one-dimensional rod. Further, there are various ways to control the shape of the dots. For example, two-dimensional dots can be made circular or rectangular. Two quantum dots can be combined in such a way that the electrons move between the dots and form a quantum dot 'molecule' [4].

The word 'quantum' in the name refers to the fact that the physics of quantum dots is described by quantum mechanics, which was developed to describe the physics of atomistic systems at the typical length scales of 10^{-9} to 10^{-10} m. In experiments quantum dots show electronic properties which are reminiscent of real atoms, despite a huge difference in size between these systems. Quantum dots have increased stability at certain electron numbers corresponding to closed-shell noble gas atoms. Hund's rules are also often followed. Therefore quantum dots are sometimes called artificial atoms. The origin of the similarities between atoms and quantum dots can be explained with quantum theory. A droplet of electrons in quantum dots must obey the uncertainty relations, the Pauli exclusion principle, and the other laws of quantum theory.

As well as being possible candidates for nanoscale electric components quantum dots have attracted a considerable theoretical interest. They are excellent model systems in studying fermionic properties of matter and testing quantum theory. The characteristic energy scale of these systems is of the order of millielectronvolts (meV) instead of electronvolts in a real atomic system. Due to the large length scale and the low energy scale relatively weak external magnetic fields can cause measurable changes in the electronic structures of the dots. In real atomic systems such changes would occur at magnetic fields well beyond those attainable in laboratory environments. Therefore, such transi-

tions and their relation to various theoretical models can be studied using quantum dots as model systems.

2.2 Fabrication methods

In the conduction bands of metals and semiconductors electrons are free to move in all three spatial directions. To trap electrons into a quantum dot we need to restrict their movement to a small volume. There are a number of ways to do this. The present work concentrates on two-dimensional (2D) quantum dots made using semiconductor interfaces, where the movement of electrons is not possible perpendicular to the interface. In terms of quantum mechanics the energy difference between the ground state and the first excited state of the momentum in perpendicular direction is very large. Therefore, transitions to these excited states are not possible in low temperatures. The movement in the remaining two spatial dimensions can be controlled by tailoring the geometry of the structure.

Semiconductor layers can be grown very accurately using techniques such as molecular beam epitaxy (MBE) or chemical vapour deposition (CVD). A semiconductor can be grown one atomic layer at a time and abrupt interfaces can be formed between materials of different band gaps, for instance GaAs and $Al_xGa_{1-x}As$. Figure 2.1 shows the energy bands at the GaAs/AlGaAs interface [5]. There is a relatively high density of electrons in the thin accumulation zone in GaAs originating from the donors in AlGaAs. The thickness of this zone is typically of the order of a few nanometers or less. This confines the movement of electrons into two dimensions. The resulting structure is known as the two-dimensional electron gas (2DEG). There is a positive depletion space-charge in the AlGaAs near the 2DEG (see figure 2.1). An undoped spacer layer of finite thickness can be further grown in between the layers of AlGaAs and GaAs to separate the ionized donors from the 2DEG. This greatly enhances the electron mobility due to the reduced impurity scattering.

The earliest man-made quantum dots were made by etching slim pillars from a large sheet of structure which contained a 2DEG. The formed structure is called a vertical quantum dot. If a voltage is applied over the structure the number of confined electrons in the dot can be controlled. The potential affecting the electrons is approximately constant inside the quantum dot and the electrons are confined inside the etched walls of the dot. Therefore a hard-wall well-like potential is a good model potential for these quantum dots. Another way to create quantum dots is to use lithographic patterning methods to form lateral quantum dots. Metal electrodes are deposited on top of the semiconductor structure which contains the 2DEG. When voltage is applied over the electrodes, electrons in the electron gas are confined. Again, the number of electrons trapped in the dot can be controlled with the voltage. In this case, the external confining potential is varying smoothly and its shape depends on the form of the deposited electrodes. Usually a parabolic potential is chosen as the model potential.

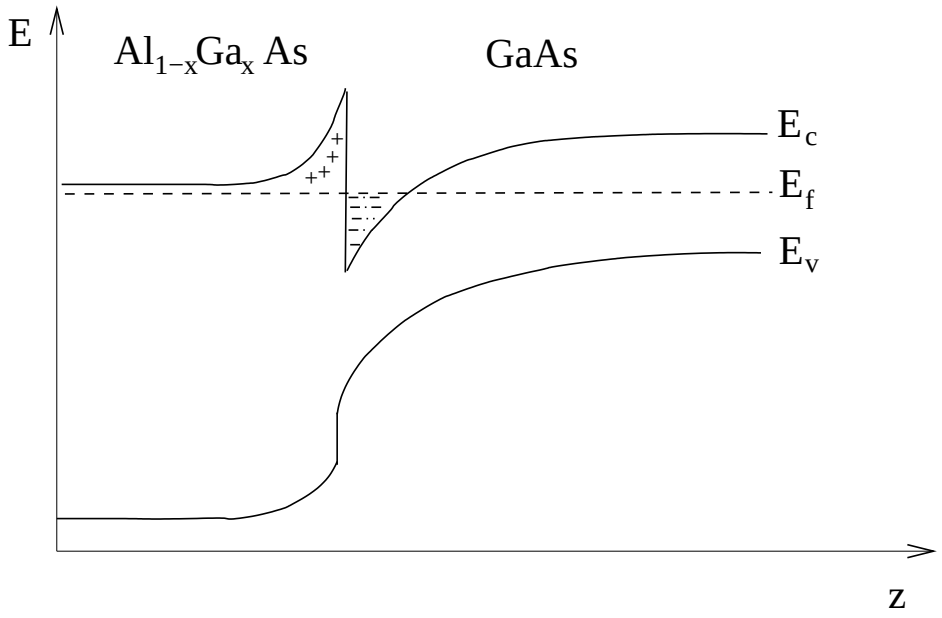

Figure 2.1: Energy bands at the semi-insulating GaAs/n-type $Al_xGa_{1-x}As$ heterostructure. The Fermi level must remain constant over the whole sample. There is a high concentration of free electrons in the space-charge zone in the GaAs, since the Fermi energy is above the conductance band minimum in this region. The ionized donors have given electrons to the energetically more favourable potential well in the accumulation zone of GaAs. This thin layer of mobile electrons at the interface region is known as the two-dimensional electron gas (2DEG). The system remains charge neutral due to the neutralizing positive depletion space-charge in AlGaAs. In theoretical models the effect of the positive space-charge can be included in the external potential of the electron gas.

2.3 Technological applications

The versatile physics of quantum dots creates a promising field of possible applications. The field effect transistors (FETs) in computers could be replaced by quantum-dot logic gates [6]. There have been proposals of using a double-dot 'hydrogen' molecule as the basic elementary gate in quantum computers [7]. In this component the electron spins are entangled and serve as the qubit.

Quantum dots can also be combined with superconductors. Numerical simulations performed in this work for the superconductor-quantum dot-superconductor (SNS) junction show that the electron-electron interactions in quantum dots affect the supercurrent. This phenomenon opens a possible way to control the supercurrent using the gate voltage of the quantum dot. Some results suggest that the interaction effects may even enhance the supercurrent. Applications of this structure include the Josephson field effect transistor and the injected current SNS transistor. The physics of these system is, however, not yet fully understood and the work is in progress.

Chapter 3

THEORETICAL BASIS

3.1 Quantum theory

The physics of quantum dots is most accurately described by quantum theory. It was conceived in the beginning of the 20th century to describe the physics of the microscopic world of atoms [8]. Up to this day there are no experiments that violate the principles of quantum theory. Therefore it is a fundamental theory of physics. After the special theory of relativity was combined with quantum theory by P.A.M. Dirac and others in the 1920's the theoretical basis of chemistry and condensed-matter physics was completed. All the chemical reactions of atoms and molecules and the structure and properties of matter can in principle be explained within the framework of quantum theory.

The basic equation for non-relativistic interacting particles in quantum mechanics is the Schrödinger equation

$$H\Psi = \left\{ \sum_{i}^{N} -\frac{\hbar^2}{2m_i}\nabla_i^2 + \sum_{i<j} V(\mathbf{r}_i - \mathbf{r}_j) + U(\mathbf{r}_i) \right\} \Psi = i\hbar\frac{\partial\Psi}{\partial t}, \tag{3.1}$$

where N is the number of particles in the system, H is the total energy operator (Hamiltonian), $\mathbf{r}_i$ are position coordinates of the particles, V is the inter-particle potential and U is the external potential [9]. The effect of external magnetic fields as well as some other details have been suppressed here but, in principle, the equation (3.1) captures all the physics of N-particle systems. The Hamiltonian is a partial differential operator which operates on the $3N$-dimensional (many-body) wave function Ψ, which is the description of a physical system and its state

$$\Psi = \Psi(\mathbf{r}_1, \mathbf{r}_2, ..., \mathbf{r}_N). \tag{3.2}$$

All the physical properties and results of the measurements can be predicted from the wave function. In the Copenhagen interpretation of quantum mechanics the wave function is the complete and only description of a physical system. There are no other entities or 'hidden variables' in nature which are not included in the wave function itself. This

leads to a probabilistic interpretation of quantum theory. The statistical transformation theory states that prior to the measurement of a physical observable the outcome of the measurement is a statistical variable and the wave function of the system exists in the superposition of several states. The measurement of the observable fixes its value and the wave function of the system transforms to correspond to the eigenstate of the observed value. The transformation theory furnishes a machinery to calculate the probability distribution of such observables from the wave function.

The mathematical formulation and the principles of quantum mechanics are known, but this does not directly allow us to understand the physical phenomena. Due to the high dimensionality of the wave function, the Schrödinger equation (3.1) can be solved exactly only in the case of very simple systems consisting of a few particles. One example of such systems is the hydrogen atom. As the number of particles in the system increases, the dimensionality of the wave function grows and an exact solution becomes quickly impossible. The analytical solutions of simple few-particle systems in some cases help us understand the physics of larger many-body systems. This is, however, not always the case. Knowing only the basic forces and the constituent particles of the system does not usually allow us to understand the physics of the system. For instance, the physics of superconductivity was not properly understood until the advent of the BCS-theory of superconductivity in the late 1950's, more than 30 years after the formulation of quantum mechanics [10]. The independent electron approximation was then abandoned and it turned out that at low temperatures the pair interaction of the electrons via the quanta of the lattice vibrations (phonons) formed a superconducting bound state, the so-called Cooper pairs. Therefore superconductivity is a true many-body phenomenon. The physics of few-particle systems cannot in this case account for the physics of complex (in this case even macroscopic) systems. This has some profound consequences for the understanding of physics. New kind of physics can emerge as the complexity of the system increases. Nobel laureate Philip Anderson coined the phrase *emergent phenomena* for this [11]. More complex systems in nature are different from systems of low complexity and it is not possible to naively extrapolate the physics of complex systems from the physics of simple systems.

These observations apply also to quantum dots. Many-body calculations of these systems reveal a rich variety of unexpected physical phenomena. These calculations offer insight to the behaviour of fermionic systems as well as a basis for possible future applications of quantum dots.

3.2 Approximations in many-body physics

The physical properties of quantum dots, *e.g.* conductivity, heat capacity and light absorption, have their origin in the complex many-body physics of constituent parts of the system, the electrons and the nuclei. The quantum theory must therefore be applied to predict and understand such phenomena. However even the smallest quantum dots contain thousands of electrons and nuclei and solving the Schrödinger equation (3.1) exactly for such systems is an impossible task since the wave function is $3N$-dimensional. Even if the wave function is discretized the amount of computer memory needed to store the wave function grows exponentially as the number of particles in the system increases.

Terabytes of computer memory would be needed to store the discretized wave function for a system of as few as 4 particles and for 20 particles the amount of memory bytes required exceeds the estimated number of atoms in the universe. Therefore, a central task in solving a physical problem is finding a suitable computational approach and plausible approximations which make the solution of the equations tractable. Such approximations must not fail to capture the essential properties of the exact but inaccessible solutions of quantum mechanical equations.

3.3 Effective-mass theory

The approximations in the calculations must obey the principles of quantum mechanics in order to be successful. Such principles are often related to the symmetries of the system under consideration. Using the group theoretical analysis it can be shown that the symmetries impose conservation laws in the system [12]. Therefore a successful approximation must preserve these conserved quantities. The most important consequences of this are the spin-statistics theorem and the Pauli exclusion principle. In quantum theory the particles are indistinguishable quanta of the fields. As a direct consequence, the wave function should not make any distinction between the different particles. It can be shown that the wave function must be antisymmetric with respect to the exchange of two particles in the notation of the wave function, if it is to describe electrons or other fermions with a half-integer spin. In the case of bosons, particles with integer spin, the wave function must be symmetric with respect to the particle exchange. In the case of fermions this symmetry leads to the Pauli exclusion principle and the Fermi-Dirac statistics. Even crude approximations which take this symmetry property into account can turn out to be very successful. The independent-electron approximation takes the Pauli exclusion principle into account, but ignores complicated electron-electron Coulomb interactions. It turns out that this elementary free-electron gas model can be readily solved for even a macroscopic system and the result gives a good picture of the metallic state of matter. We now turn our attention to an extension of this this model since it provides us the effective-mass theory which will be used throughout the present work.

Metals and semiconductors are ordered systems, where atoms are arranged in a fixed lattice structure and at least some of atom's electrons (or holes) are generally free to move in all three spatial directions [13]. These electrons are referred to as conduction or valence electrons. The mass of the electron is much smaller than the mass of an ion so the electrons move faster and the electron distribution in metals usually relaxes very fast after even the slightest changes in the positions of the nuclei. Therefore we can in most cases assume that the electron distribution is in the ground state of the current ion distribution. This is known as the adiabiatic or Born-Oppenheimer approximation [14]. At low temperatures the electrons and the ions can then be treated separately and we can assume that the position of the ions are fixed. This approximation usually greatly simplifies the electronic structure calculations, but it ignores the interaction effects between the dynamics of a lattice of ions and the electrons. For instance, in metals these effects become noticeable at low temperatures when the interactions of the quanta of lattice vibrations and the electrons may give rise to superconductivity.

The electrons in valence shells of metals and semiconductors are moving in a periodic

potential of the lattice of charged ions. By taking the Fermi-Dirac statistics into account and ignoring the electron-electron interactions we can analyze the movement of the semi-classical electrons in this periodic potential. This analysis results in a remarkably good picture for metals. The wave functions of such electrons can be shown to be Bloch waves. Due to the periodic potential these electrons have an *effective mass* m^*, which usually depends on the kinetic energy of the electron. If m^* turns out to be approximately a constant, the problem of calculating the electronic structure is greatly simplified. This collection of approximations is known as the effective-mass theory. This model will be used in this work to describe the electrons in the 2D electron gas. For GaAs m^* is 0.067 times the mass of a free electron.

3.4 Electrons in 2D electron gas

An approximate condition where quantum effects become non-negligible can be obtained from the Fermi wave length λ_{F} of the electron, which is the wavelength of the most energetic electrons. In metals, where valence electrons are free to move in all three spatial directions, the Fermi energy is of the order of several electronvolts. Therefore λ_{F} is very small for metals and is of the order of 0.5 nm.

For 2D electron gas in semiconductor heterostructures the Fermi wave length is larger than that for metals. Define the coordinate system so that x and y are parallel to the plane of 2D electron gas and z is perpendicular to this plane. The kinetic energy of the electrons can be approximated as

$$E_{\mathrm{kin}} = \frac{\hbar^2}{2m^*}k_x^2 + \frac{\hbar^2}{2m^*}k_y^2, \tag{3.3}$$

where m^* is the effective mass of the electron (approximated to be the same in both x and y directions). Since the density of states is energy independent for 2D electron gas, the electron density n and the Fermi energy E_{F} are linearly related. For GaAs we get [13, 15]

$$n = m^* E_{\mathrm{F}}/\pi\hbar^2. \tag{3.4}$$

Combining (3.3) and (3.4) we get for GaAs Fermi wavelength which is of the order of 40 nm. [15]. The corresponding Fermi energy is about 13 meV. In the particle-in-a-box picture the energy in the confined z dimension is quantized to

$$E_z(n_i) = \frac{\hbar^2\pi^2 n_i^2}{2m^* d^2}, \tag{3.5}$$

where $n_i = 1, 2, 3, ...$ and d is the thickness of the layer. This energy corresponds to the energy levels in the infinite quantum well. For a 10 nm thick layer of GaAs, $E_z(1) \simeq$ 50 meV showing that there are no excitations in the z direction if the layer is thin enough. Since the Fermi wave length is of the order of the size of the quantum dot, quantum mechanics must be applied to obtain the correct physical description of the droplets of charge in these structures.

Chapter 4

VARIATIONAL QUANTUM MONTE CARLO METHOD

The expectation values of quantum mechanical observables can be calculated from the state vector Ψ using the equation

$$\langle \hat{O} \rangle = \frac{\langle \Psi | \hat{O} | \Psi \rangle}{\langle \Psi | \Psi \rangle}, \tag{4.1}$$

where $\hat{O}$ is the operator which corresponds to the observable in question. The *variational principle* states that for an arbitrary state vector Ψ' the expectation value for the Hamiltonian operator is always greater than or equal to that for the ground state Ψ_0. Denoting E as the energy eigenvalue of the ground state

$$E \leq E' = \frac{\langle \Psi' | \hat{H} | \Psi' \rangle}{\langle \Psi' | \Psi' \rangle}. \tag{4.2}$$

The inner product in the equation (4.1) is an integral in the $3N$-dimensional space of the wave function. The convergence of the conventional numerical integration schemes like the trapezoidal rule and the Simpson's rule strongly depends on the dimensionality of the integration space. In two-dimensional or three-dimensional space these schemes work well and give accurate results, but the convergence becomes increasingly slow in higher space dimensions which renders these methods unusable to evaluate the integrals in equation (4.1). It can be shown that in high-dimensional spaces the Monte Carlo method is a more efficient means for estimating the integrals. The Monte Carlo method is a collection of techniques which utilize statistical random sampling to get approximate solutions of mathematical problems [16,17]. It can be applied to the numerical integration of the integrals in the equation (4.1). Unlike the conventional numerical integration quadratures, the Monte Carlo method converges at the same rate in any dimension. Therefore it is well suited for the calculation of high-dimensional integrals in the equation (4.1). This numerical integration technique combined with the variational principle (formula (4.2)) is the basis of the variational quantum Monte Carlo method.

The variational quantum Monte Carlo method (VMC) [16] is a computational approach for approximating the many-body wave function Ψ and the associated eigenvalues. A trial wave function Ψ' is chosen with a set of parameters that can be adjusted so that E' in the formula (4.2) is minimized. E' is approximated by using statistical sampling in the numerical evaluation of the $3N$-dimensional integrals. The result of this minimization is then taken as the approximation for the true ground-state wave function Ψ with the associated energy eigenvalue E. In many-body physics the success of this approach depends on the choice of the trial wave functions and the parametrization. However the variational principle (4.2) guarantees that the approximation of the ground-state energy E' cannot be less than the true ground state energy E.

Chapter 5

DENSITY-FUNCTIONAL APPROACH

The density-functional theory (DFT) for the solution of many-body problems in physics and chemistry was in its earliest form proposed by Hohenberg, Kohn and Sham in the 1960's [18, 19]. It is based on the *mean-field* approach, *i.e.*, electrons are considered one at a time in the one-particle picture and the effect of the other electrons is averaged out and included in an *effective* potential felt by each electron. This leads to Kohn-Sham equations which include an effective one-particle Schrödinger equation and rules on calculating the electron density and the effective potential.

The density-functional theory has turned out to be one of the most successful computational methods in condensed-matter physics. It can predict the electronic structures of atoms, molecules, solids, and semiconductors with good accuracy. It is also applicable to time-dependent systems within the framework of the time-dependent density-functional theory (TDDFT). The DFT is an especially powerful method when dealing with large systems of tens or hundreds of particles. For his pioneering work with DFT, Walter Kohn was awarded the Nobel price in chemistry in 1998.

The cornerstone of the density-functional theory is the Hohenberg-Kohn theorem [18], which states that even if the wave function is $3N$-dimensional, the *ground-state* properties of the system are determined by the particle density alone. This is a remarkable simplification since the ground-state properties can, in principle, be calculated using the much simpler three-dimensional particle density instead of the complicated $3N$-dimensional wave function. Later, the density-functional theory has been extended to excited states for which a generalization of the Hohenberg-Kohn theorem can be introduced [20].

5.1 Spin-density-functional theory

The original density-functional theory did not take into account the effects of a non-zero spin-polarization and currents induced by *e.g.* an external magnetic field. In open-shell

atoms, ferromagnetic systems, and systems in an external magnetic field there are finite spin and current densities in the ground state of the system. Through the work by Gunnarsson and Lundqvist and that by von Barth, the density-functional theory was generalized for systems with non-zero spin-polarization in the spin-density-functional theory (SDFT) [21, 22]. Later, however, it was shown that the potentials in this theory are not necessarily unique functionals of the spin densities [23, 24]. As a consequence there exists no extension of the Hohenberg-Kohn theorem in the SDFT, which casts a shadow on the generality of this theory. Despite this weakness the SDFT has been successfully applied to systems exhibiting broken spin symmetry.

The Hamiltonian for a system of N non-relativistic electrons moving in the scalar potential V_{ext} and vector potential $\mathbf{A}$ can be written in the effective-mass theory as [1]

$$H = \frac{1}{2m^*}\sum_{i=1}^{N}\left[-i\hbar\nabla_i + e\mathbf{A}(\mathbf{r}_i)\right]^2 + \frac{1}{2}\frac{1}{4\pi\epsilon}\sum_{i\neq j}\frac{e^2}{|\mathbf{r}_i-\mathbf{r}_j|} + \sum_{i=1}^{N}V_{\text{ext}}(\mathbf{r}_i). \tag{5.1}$$

From this, the self-consistent Kohn-Sham equations can be derived. They include the Poisson equation for the solution of the Hartree potential V_{H}, *i.e.* the Coulomb potential for the electronic charge density n,

$$\nabla^2 V_H = -\frac{n}{\epsilon}, \tag{5.2}$$

where ϵ is the dielectric constant of the medium. Moreover, the equation for spin densities is

$$n_\sigma(\mathbf{r}) = \sum_{i}^{N_\sigma}|\psi_{i,\sigma}(\mathbf{r})|^2, \tag{5.3}$$

where $\sigma = \uparrow, \downarrow$ is the spin index, N_σ is the number of electrons in the spin direction σ and $\psi_{i,\sigma}$'s are the one-particle wave functions. The summation is over the N_σ lowest states in energy. Finally, the Schrödinger equation for one-particle wave functions of the system

$$\left\{\frac{1}{2m^*}\left[\mathbf{p}+e\mathbf{A}(\mathbf{r})\right]^2 + V_{\text{eff},\sigma}(\mathbf{r})\right\}\psi_{i,\sigma} = \epsilon_{i,\sigma}\psi_{i,\sigma}. \tag{5.4}$$

The *effective* scalar potential

$$V_{\text{eff},\sigma}(\mathbf{r}) = V_{\text{ext}}(\mathbf{r}) + V_{\text{H}}(\mathbf{r}) + V_{\text{xc},\sigma}(\mathbf{r}) + V_{\text{Z}} \tag{5.5}$$

consists of the external scalar potential V_{ext}, Hartree potential V_{H}, the exchange-correlation potential V_{xc} and the Zeeman-term $V_Z = g^*\mu_B B s_\sigma$, where μ_B is the Bohr magneton, $s_\sigma = \pm 1/2$, B is the magnetic field and g^* is the gyromagnetic ratio. The Hartree potential contains a spurious Coulomb self-interaction potential of each electron with itself. This spurious potential is partially removed by the self-interaction part of the exchange-correlation potential. In the calculations usually more than N states are solved by introducing an occupation number for each state of the system. This allows calculations at finite temperature. In the case of electrons and other fermions the occupation numbers are between 0 and 1, and they are obtained from the Fermi-Dirac distribution.

[1] The equations are given in SI-units. $e = +1.602 \cdot 10^{-19}$C is the (absolute) charge of electron.

The Kohn-Sham equations are usually solved by minimizing the total energy functional directly or by a self-consistent iteration procedure. The iterations start with an initial guess for the effective potential for which the one-particle states of the system are solved. Then the electron densities are calculated using the equation (5.3) and a new effective potential is calculated using the equations (5.2) and (5.5). This procedure is repeated until a converged self-consistent solution for the Kohn-Sham equations is obtained.

5.1.1 Exchange-Correlation functional

The SDFT ignores effects of currents induced into the system by the external magnetic field $\mathbf{B}$. Therefore, $V_{\rm xc}$ depends only on the spin densities. In general the exchange-correlation potential $V_{\rm xc}$ depends on the symmetries of the system. In the absence of a recipe on how to choose this $V_{\rm xc}$ in the actual calculations $V_{\rm xc}$ is usually taken as the exchange-correlation potential of the uniform electron-gas. In the local spin-density approximation (LSDA) $V_{\rm xc}$ is taken to be a local function of the spin densities,

$$V_{{\rm xc},\sigma}(n_\uparrow(\mathbf{r}), n_\downarrow(\mathbf{r})) = \frac{\partial(n e_{\rm xc}(n_\uparrow(\mathbf{r}), n_\downarrow(\mathbf{r})))}{\partial n_\sigma(\mathbf{r}).}, \tag{5.6}$$

where $n_\uparrow$ and $n_\downarrow$ are the spin-up and spin-down densities, respectively, and $e_{\rm xc}(n_\uparrow, n_\downarrow)$ is the exchange-correlation energy per electron in the homogeneous electron gas. The total exchange correlation energy in the LSDA is then

$$E_{\rm xc} = \int e_{\rm xc}(\mathbf{r}) n(\mathbf{r}) d\mathbf{r}. \tag{5.7}$$

Tanatar and Ceperley performed diffusion quantum Monte Carlo simulations for the 2D electron gas and obtained a functional for $e_{\rm xc}$ that has been widely used [25]. Defining polarization $\xi = (n^\uparrow - n^\downarrow)/n$ and $x = \sqrt{m^*}e/[\hbar(\pi n)^{1/4}]$, the functional is written as

$$e_{\rm xc}^{\rm TC} = e_{\rm x}(x,\xi) + e_{\rm c}(x,\xi) = \frac{me^4}{2\hbar^2}\left[\frac{1+\xi^2}{x^4} - \frac{4\sqrt{2}}{3\pi x^2}\left[(1+\xi)^{3/2} + (1-\xi)^{3/2}\right]\right] + e_{\rm c}(x,\xi), \tag{5.8}$$

$$e_{\rm c}(x,\xi) = a_0 \frac{1 + a_1 x}{1 + a_1 x + a_2 x^2 + a_3 x^3}, \tag{5.9}$$

where $a_i(\xi)$'s are ξ-dependent parameters, and $e_{\rm x}$ and $e_{\rm c}$ are the exchange and correlation parts of the energy, respectively[2]. Tanatar and Ceperley performed Monte Carlo calculations only for spin-compensated ($\xi = 0$) and spin-polarized ($\xi = 1$) systems [25]. For the correlation potential in intermediate polarizations the Tanatar-Ceperley data is often used with the exchange-like interpolation [26]

$$e_{\rm c}(x,\xi) = e_{\rm c}(x,\xi=0) + \frac{(1+\xi)^{3/2} + (1-\xi)^{3/2} - 2}{2^{3/2} - 2}[e_{\rm c}(x,\xi=1) - e_{\rm c}(x,\xi=0)]. \tag{5.10}$$

[2]The exchange-correlation energy is in SI-units. The numerical value for a_0 (not given here) depends on the chosen system of units. Tanatar and Ceperley used in their work Rydbergs for the unit energy and Bohr radius for the unit of length.

Recently, Attaccalite, Moroni, Gori-Giorgi, and Bachelet made fixed-node diffusion quantum Monte Carlo calculations for the 2D electron gas with improved accuracy and proposed a new analytic representation of the correlation energy [27, 28]. The exchange-correlation energy reads now as

$$e_{\mathrm{xc}}(r_s,\xi) = e_{\mathrm{x}}(r_s,\xi) + (e^{-\beta r_s}-1)e_{\mathrm{x}}^{(6)}(r_s,\xi) + \alpha_0(r_s) + \alpha_1(r_s)\xi^2 + \alpha_2(r_s)\xi^4. \quad (5.11)$$

The exchange energy e_{x} is the same as in the equation (5.8) and $r_s = m^* e^2/(\sqrt{\pi n}\hbar^2)$ is the dimensionless density parameter. In the equation (5.11), $e_{\mathrm{x}}^{(6)}$ contains the terms of the Taylor expansion of e_{x} with respect to ξ at $\xi = 0$ which are beyond the fourth order in ξ, α's are density dependent functions of the generalized Perdew-Wang form [29], and $\beta = 1.3386$. Compared to the work by Tanatar and Ceperley there are a number of improvements in the numerical calculations. For instance, so called backflow correlations in many-body wave functions have been included, and infinite size extrapolations have been performed in the Monte Carlo data.

5.2 Current-spin-density-functional theory

In the spin-density-functional theory the exchange-correlation potentials do not depend on the currents induced into the system. The effect of these currents on the exchange-correlation energy is non-negligible if the applied magnetic field is large. To overcome this problem Vignale and Rasolt presented the current-spin-density-functional theory for electronic systems in arbitrary strong magnetic fields in 1988 [30].

5.2.1 Kohn-Sham equations

Consider a 2D system of electrons in the effective-mass theory. The electrons are moving in an external scalar potential $V_{\mathrm{ext},\sigma}(\mathbf{r})$ and a homogeneous external magnetic field perpendicular to the movement of the electrons. A set of self-consistent single-particle equations can be derived in the CSDFT. In the SI-units they can be written as

$$\left(\frac{1}{2m^*}\left[-i\hbar\nabla + e[\mathbf{A}(\mathbf{r}) + \mathbf{A}_{\mathrm{xc},\sigma}(\mathbf{r})]\right]^2 + \frac{e^2}{2m^*}[A^2(\mathbf{r}) - [\mathbf{A}(\mathbf{r}) + \mathbf{A}_{\mathrm{xc},\sigma}(\mathbf{r})]^2] \right.$$
$$\left. + V_{\mathrm{ext},\sigma}(\mathbf{r}) + V_H(\mathbf{r}) + V_{\mathrm{xc},\sigma}(\mathbf{r})\right)\psi_{i,\sigma}(\mathbf{r}) = \epsilon_{i,\sigma}\psi_{i,\sigma}(\mathbf{r}), \quad (5.12)$$

where σ is the spin index, i is the state index, $V_{\mathrm{xc},\sigma}$ is the exchange-correlation scalar potential, V_H is the Hartree potential, $\mathbf{A}$ is the vector potential of the external magnetic field, $\mathbf{A}_{\mathrm{xc},\sigma}$ is the exchange-correlation vector potential, $\psi_{i,\sigma}$ are the one-particle wave functions and $\epsilon_{i,\sigma}$ are the corresponding energy eigenvalues. The Zeeman term V_{Z} can be included in the external scalar potential (see section 5.1.1). By collecting the scalar terms in the brackets in the equation (5.12), the *effective* scalar potential can be defined as

$$V_{\mathrm{eff},\sigma} = \frac{e^2}{2m^*}[A^2(\mathbf{r}) - [\mathbf{A}(\mathbf{r}) + \mathbf{A}_{\mathrm{xc},\sigma}(\mathbf{r})]^2] + V_\sigma(\mathbf{r}) + V_H(\mathbf{r}) + V_{\mathrm{xc},\sigma}(\mathbf{r}) + V_{\mathrm{Z}}. \quad (5.13)$$

Quantity	Before transformation	After transformation
Vector potential	$\mathbf{A}(\mathbf{r})$	$\mathbf{A}(\mathbf{r}) - \nabla\Lambda(\mathbf{r})$
Effective scalar potential	$V_{\mathrm{eff},\sigma}(\mathbf{r})$	$V_{\mathrm{eff},\sigma}(\mathbf{r})$
Exchange and correlation energy	$e_{\mathrm{xc},\sigma}(\mathbf{r})$	$e_{\mathrm{xc},\sigma}(\mathbf{r})$
One-particle wave functions	$\psi_{i,\sigma}(\mathbf{r})$	$\exp(ie\Lambda/\hbar)\psi_{i,\sigma}(\mathbf{r})$
Spin density	$n_\sigma(\mathbf{r})$	$n_\sigma(\mathbf{r})$
Paramagnetic current density	$\mathbf{j}_\mathrm{p}(\mathbf{r})$	$\mathbf{j}_\mathrm{p}(\mathbf{r}) + en(\mathbf{r})\nabla\Lambda(\mathbf{r})/m^*$
Physical current density	$\mathbf{j}(\mathbf{r})$	$\mathbf{j}(\mathbf{r})$
Total energy	E_tot	E_tot

Table 5.1: Transformation of self-consistent quantities in the CSDFT when another gauge is used for the vector potential. The physical observables are gauge invariant.

The generalized Hohenberg-Kohn theorem [30] can be formulated using the paramagnetic current density defined as

$$\mathbf{j}_\mathrm{p}(\mathbf{r}) = \sum_{i,\sigma} -\frac{i\hbar}{2m^*}\left\{\psi^\dagger_{\sigma,i}\nabla\psi_{\sigma,i} - \psi_{\sigma,i}\nabla\psi^\dagger_{\sigma,i}\right\}. \tag{5.14}$$

The physical current density $\mathbf{j}$ is related to the paramagnetic current density $\mathbf{j}_\mathrm{p}$ by the equation

$$\mathbf{j}(\mathbf{r}) = \mathbf{j}_\mathrm{p}(\mathbf{r}) + \frac{e}{m^*}n(\mathbf{r})\mathbf{A}(\mathbf{r}). \tag{5.15}$$

The generalized Hohenberg-Kohn theorem now states that in the CSDFT the ground state is uniquely determined by the paramagnetic current density and the spin densities. Therefore the CSDFT is constructed using the paramagnetic current density in the exchange-correlation energy functional. The ground state, however, is not a unique functional of the *physical* current density. The consequences of this problem are not yet fully understood [24].

5.2.2 Gauge invariance

The vector potential is chosen so that it corresponds to the external magnetic field $\mathbf{B}$ via the relation $\mathbf{B}(\mathbf{r}) = \nabla\times\mathbf{A}(\mathbf{r})$. A widely used form for the vector potential corresponding to the uniform magnetic field along the z-axis is $\mathbf{A}(\mathbf{r}) = \frac{1}{2}B(-y\mathbf{i} + x\mathbf{j})$. This is not the unique solution for the vector potential. It can be shown that the magnetic field is invariant under the gauge transformation defined as $\mathbf{A}(\mathbf{r}) \to \mathbf{A}(\mathbf{r}) - \nabla\Lambda(\mathbf{r})$, where Λ is an arbitrary function. Therefore the physical measurable quantities should not depend on the chosen gauge if the theory is physically sound. In table 5.2.2 the transformations of the quantities in the CSDFT are shown. It should be noted that the paramagnetic current density $\mathbf{j}_\mathrm{p}$ is *not* invariant. The physical current density on the other hand is gauge invariant as well as the other observable quantities, the total energy and the particle densities. This means that the CSDFT satisfies the gauge invariance.

5.2.3 Exchange-correlation functional in finite magnetic field

In the CSDFT e_{xc} is a functional of n, ξ and $\mathbf{j}_{\mathrm{p}}$. It can be shown [30] that in the lowest order *local* approximation the exchange-correlation energy density is a local function of the electron density, the polarization and a quantity called vorticity, which is defined as z-component of $\nabla \times (\mathbf{j}_{\mathrm{p}}/n)$, *i.e.*

$$\gamma = \nabla \times \frac{\mathbf{j}_{\mathrm{p}}(\mathbf{r})}{n(\mathbf{r})}\bigg|_z . \tag{5.16}$$

Then, explicitly, $e_{\mathrm{xc}} = e_{\mathrm{xc}}(n(\mathbf{r}), \xi(\mathbf{r}), \gamma(\mathbf{r}))$. The exchange-correlation scalar potential V_{xc} is obtained in the local approximation by calculating the functional derivative

$$V_{\mathrm{xc},\sigma}(n_\uparrow, n_\downarrow, \gamma) = \frac{\partial(n e_{\mathrm{xc}})}{\partial n_\sigma .} \tag{5.17}$$

The exchange-correlation vector potential $\mathbf{A}_{\mathrm{xc}}$ depends on the derivative of the e_{xc} with respect to the vorticity. The x and y components of the $\mathbf{A}_{\mathrm{xc}}$ are

$$A_{\mathrm{xc},x} = \frac{1}{n}\frac{\partial}{\partial y}\frac{\partial(n e_{\mathrm{xc}})}{\partial \gamma}, \tag{5.18}$$

$$A_{\mathrm{xc},y} = -\frac{1}{n}\frac{\partial}{\partial x}\frac{\partial(n e_{\mathrm{xc}})}{\partial \gamma}. \tag{5.19}$$

Therefore, the contribution of the exchange-correlation energy to the total energy depends on the value of e_{xc} at the given spin densities and vorticity *and* its derivatives with respect to both spin densities and the vorticity.

The accuracy of the CSDFT depends strongly on a suitable choice of the exchange-correlation functional. The exact form for this is not known and a poor choice for e_{xc} can lead to significant errors in the results. Approximate forms can be obtained by using the simulation data for the homogeneous 2D electron gas. If the effect of currents can be assumed small the exchange-correlation vector potential $\mathbf{A}_{\mathrm{xc}}$ can be neglected and the Kohn-Sham equations of the CSDFT reduce to those of the SDFT. Therefore the limit of e_{xc} in zero-field can be taken as the exchange-correlation functional of the 2D electron gas in the zero field (see section 5.1).

The vorticity dependence in the high magnetic field-limit can be obtained using the results by Levesque, Weis, and MacDonald [31].

$$e_{\mathrm{xc}}^{\mathrm{LWM}}(n, \gamma) = -0.782133\sqrt{2\pi n}\left(1 - 0.211\nu^{0.74} + 0.012\nu^{1.7}\right), \tag{5.20}$$

where $\nu = 2\pi n/\gamma$ is the Landau-level filling factor[3]. Data for the totally polarized 2D electron gas in magnetic fields can be found in the works by Fano and Ortolani [32], and by Price and Das Sarma [33]. Several interpolation schemes between the high and low vorticity values have been suggested [34–36]. Ferconi and Vignale applied a Padé

[3] Effective atomic units (see section 6.3) are used in this section for easier comparison with the original papers.

approximant, fitting the high γ limit by Levesque and coworkers to the zero magnetic field functionals [37], *i.e.*,

$$e_{\rm xc}^{\rm PADE}(n,\xi,\nu) = (e_{\rm xc}^{\rm LWM}(n,\nu) + \nu^4 e_{\rm xc}^{B=0}(n,\xi))/(1+\nu^4), \tag{5.21}$$

Koskinen and coworkers fitted their functionals to the data by Fano and Ortolani and used the following formula for the interpolation to the zero-field limit [36]

$$e_{\rm xc}^{\rm K}(n,\xi,\nu) = -0.782\sqrt{2\pi n}e^{-f(\nu)} + e_{\rm xc}^{B=0}(n,\xi)(1-e^{-f(\nu)}), \tag{5.22}$$

where $f(\nu) = 1.5\nu + 7\nu^4$. These interpolation forms differ especially in the region where ν is of the order of 1. This is because simulation data for the 2D electron gas in this region is scarce and data for the partially polarized 2D electron gas is missing. This hampers the establishing of accurate interpolation forms between the low and high magnetic field limits.

5.3 Symmetry breaking

According to quantum mechanics, the wave function of the system should reflect the symmetries of the Hamiltonian. Therefore the electron density in the rotationally symmetric potential should also be rotationally symmetric. Jahn and Teller, however, found out in an early work in molecular systems that rotational symmetry can be broken [38]. Their conclusion is the Jahn-Teller theorem which states that any non-linear molecular system in a degenerate electronic state will be unstable and will undergo distortion to form a system of a lower symmetry and reduce energy by removing the degeneracy.

Similar solutions that break rotational symmetry both in the particle and spin densities can be found in the density-functional studies of quantum dot systems. An on-going discussion is whether they are artifacts of the mean-field theory or if they have a special meaning. Reimann and Manninen pointed out that symmetry-breaking solutions can be rotated by an arbitrary angle and the solution is still an equivalent solution. Therefore, the symmetry-violating solution can be considered as an intrinsic state of the system [39].

Symmetry-breaking solutions arise in the density-functional studies of quantum dot systems in a wide variety of contexts. Quantum dots in parabolic confinement potentials show spin-density wave (SDW) and charge-density wave (CDW) type solutions. They can be found especially in high magnetic fields. In the spin-density-functional studies of double-dot systems, the breaking of the spin symmetry leads to the lowering of the total energy and the solution is closer to the exact energy than that of the symmetry-preserving density-functional solution. Therefore, this symmetry-breaking solution reflects the many-body properties of the inaccessible many-body wave function.

Broken rotational symmetry in the spin densities can also be found to arise due to the mixing of states of different total spin (S) and the total angular momentum (L) quantum numbers. Only the z-component of the total spin can be specified in the local approximations in the density-functional theories. The total spin is an unknown quantity in these formalisms. According to Hirose and Wingreen [40] the solution of the Kohn-Sham equations is a state which is a mixture of several eigenstates corresponding to different S and L quantum numbers and the resulting spin densities break the rotational symmetry of the problem.

Chapter 6

NUMERICAL METHODS

6.1 Real space approach

The density-functional theories can be formulated in real space or in momentum space (k-space). For actual calculations with computers the chosen space must be discretized using a finite set of points to represent the wave function and other quantities. In the real-space formulation the values of functions are directly given in the real space grid points. In the momentum space formulation the values correspond to the amplitudes of the plane-wave components, which are eigenfunctions of the momentum operator for zero potential. Fourier transformations can be used to transform the momentum space values to real-space values and the other way round. In the actual calculations this is done using the Fast Fourier Transformation (FFT) algorithm.

In the momentum-space representation the plane-wave components are periodic functions $e^{i\mathbf{k_i}\cdot\mathbf{r}}$ in real space. Therefore, only periodic functions can be represented using this basis. In consequence, the system in the calculations is an infinite lattice. If the actual system is finite, this may cause inaccuracy in the calculations. The real-space representation is more flexible as it allows a free selection of the boundary conditions at the edges of the calculation region. Finite systems can therefore be easily modeled by setting the wave function to zero at the boundaries.

The solution of the discretized Kohn-Sham equations in real space is the most time consuming part of the density-functional calculations. For a review of real space solving techniques in density-functional theories see *e.g.* reference [41]. In the finite difference method (FD) the derivatives in the Kohn-Sham equations are converted to difference operators. The discretizations used in the present electronic structure calculations are of the 4th order in the grid spacing. Therefore they are sufficiently accurate to be used in grids of reasonable sizes. The Kohn-Sham Schrödinger equation then becomes a discretized eigenproblem

$$Hu = \lambda Bu, \tag{6.1}$$

where H and B are matrix operators, u is the solution vector and λ is the energy eigenvalue. A similar discretization can be made for the Poisson equation (equation (5.2)) or V_H can be directly calculated using numerical integration.

The discretized kinetic energy operator (∇^2-operator) usually underestimates the true kinetic energy [41]. Therefore the total kinetic energy is *lower* than that at the limit of the infinitely fine grid. Consequently the variational principle (4.2) is lost. In the plane wave methods this does not occur because the plane waves are eigenstates of the kinetic energy operator. To estimate the error in the real space calculations it is usually necessary to perform the same calculation with different grid sizes and then extrapolate the results to an infinite grid size by using *e.g.* Richardson extrapolation [42]. This usually leads to a fairly good error estimate. There are propositions for difference operators which give an upper bound estimate of the derivative and thus preserve the variational principle [43]. However, in the tests such schemes are found to be less accurate compared to the conventional finite-difference methods [44].

6.2 Rayleigh quotient multigrid method

Elementary solvers for the equation (6.1) use relaxation iteration algorithms or the conjugate-gradient method. These methods are very uneconomical if high accuracy of the solution is pursued. More advanced solvers in real space are based on the multigrid approach. The main idea of the multigrid approach is to use simple relaxation methods, such as the Jacobi iteration or the Gauss-Seidel iteration, in grids of fine and coarse spacing [45]. The Gauss-Seidel iteration is a simple iteration method and uses only the data of the near lying grid points so that the propagation of the information from one side of the grid to the other takes a large number of iterations in the fine grids. This leads to the critical slowing down phenomenon (see figure 6.1). Relaxation iteration methods in the fine grid quickly eliminate the high-frequency (short wavelength) part of the error but the convergence is very slow for the low-frequency components. The problem is overcome by using several grids with different grid spacings. The low-frequency part of the error is eliminated by projecting the solution of the fine grid to a coarse grid and performing relaxation iterations in this grid. Since the grid spacing is now larger, the low-frequency part of the error in the fine grid has a relatively higher frequency in the coarse grid and the error can now be eliminated using the Gauss-Seidel iteration. Interpolation schemes are used to inject the solution back to the fine grid to correct again for the high-frequency part of the error. Successive iterations in the different grids lead to an accurate solution in a fraction of computer time that is needed for the conjugate-gradients methods. It is also possible to refine the grid in the regions where greater accuracy is needed. The multigrid solvers are also suitable for parallel computing, which makes them powerful computational tools.

In this work the Rayleigh quotient multigrid (RQMG) solver was used for the solution of the discretized Kohn-Sham Schrödinger equation [46]. It uses the variational principle (4.2), which states that the true solution of the discretized eigenproblem of the equation (6.1) is obtained by minimizing the Rayleigh quotient,

$$\frac{\langle u|H|u\rangle}{\langle u|B|u\rangle}. \tag{6.2}$$

RQMG was originally developed to find the lowest eigenenergy and the ensuing eigenfunction [47], but the method has been extended to the simultaneous solution of several

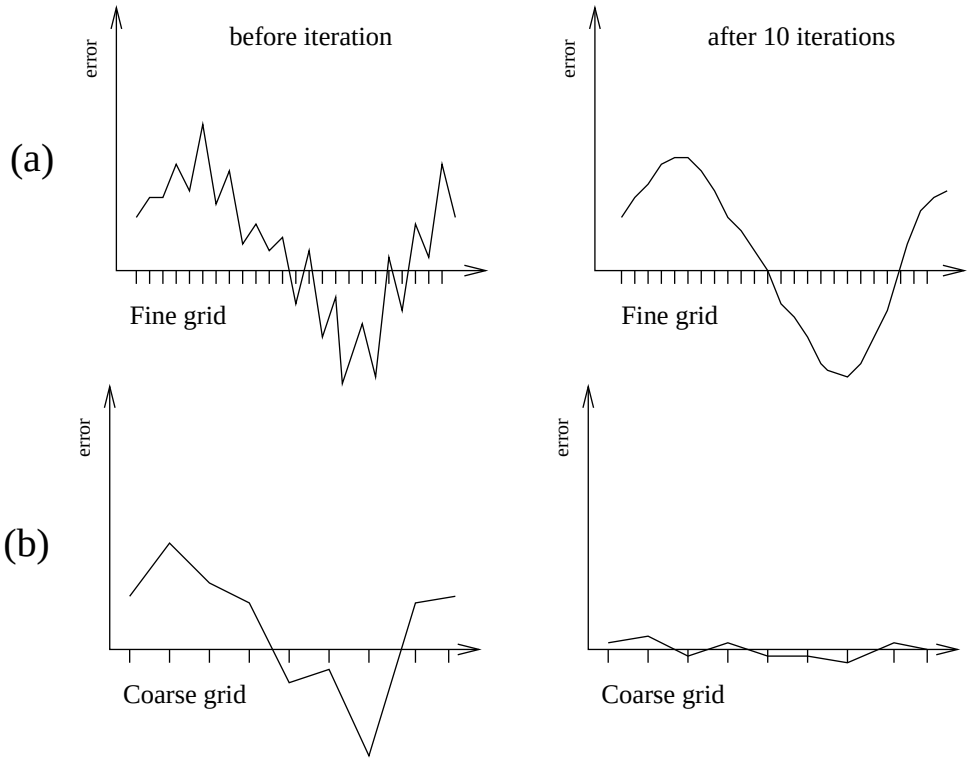

Figure 6.1: Critical slowing down of the Gauss-Seidel relaxation iteration. a) In the fine grid Gauss-Seidel iteration removes the high-frequency component of the error fast but leaves the low-frequency part of the error nearly intact. The main contributing component of the error has a periodicity of about 24 grid spacings in the picture on the right hand side. b) If the coarse grid is used for the same problem the low frequency part of the error has a periodicity of about 8 grid spacings only and the Gauss-Seidel method eliminates the error fast. Combination of iterations in the coarse and fine grids leads to fast convergence and good accuracy.

lowest eigenstates [46]. In the calculations all the states below the Fermi level and a few states above the Fermi level are solved using the RQMG solver. This allows a finite temperature to be applied to the system in order to stabilize the self-consistency iteration.

6.3 Effective atomic units

The effective-mass approximation leads to new natural units of physical quantities, which simplifies the formulas in the numerical work. Setting the effective mass $m^* = 1$ and the dielectric constant of the medium $\epsilon = 1$, Plancks constant $\hbar = 1$ and the absolute charge of the electron $e = 1$ in the CGS-unit system, we get the effective atomic units. Then the units of length, energy and magnetic field change according to the following formulae. If the Bohr radius is denoted by $a_B = \hbar^2/(me^2) = 0.529 \times 10^{-10}$ m and the unit of energy, Hartree, is Ha $= \hbar^2/(m_e e^2) = 27.2116$ eV, then the effective unit of length is $a_B^* = \epsilon a_B/m^*$ and the effective unit of energy is Ha$^* = m^*/\epsilon^2$ Ha. For GaAs $\epsilon = 12.4\epsilon_0$ and $m^* = 0.067 m_e$, so that $a_B^* \approx 9.79$ nm and Ha$^* = 3.622 \times 10^{-4}$ Ha. Therefore typical energies of electrons moving in GaAs lattice are of the order of meVs.

The unit of time is $m_e a_B^*/\hbar = 2.4189 \times 10^{-17}$s, which gives $c = 137.036$ for the velocity of light. For the unit of effective magnetic flux density the conversion formula

$$1\mathrm{T} = 4.254 \times 10^{-6} \epsilon^2/(m^*)^2 \ \mathrm{T}^* \tag{6.3}$$

can be derived using the fact that the unit of $B^2 r^2 e^2/m^*$ is the unit of energy, where r is the distance. In the CGS-units the velocity is scaled with c (see [48], Appendix A). and the above energy is written as $B^2 r^2 e^2/m^* c^2$. c is incorporated in the definition of T^* in (6.3). The coupling of the electron spin to the external magnetic field gives rise to the Zeeman energy. In effective atomic units the Zeeman energy is $E_\mathrm{Z} = \frac{1}{2} g^* s_\sigma B(T^*) m^*$ Ha*, where $s_\sigma = \pm 1/2$ and $g^* = -0.44$ is the gyromagnetic ratio in GaAs [49].

Effective atomic units are used in the numerical calculations in this work and the results will often be given in those units.

Chapter 7

PHYSICAL PHENOMENA IN QUANTUM DOT SYSTEMS

In this work physical phenomena in quantum dot systems are studied theoretically using the computational approaches presented in the previous chapters. The systems under consideration are quantum dots in the heterostructure of the GaAs/AlGaAs interface. The model for such quantum dots is the system of interacting electrons in the effective-mass approximation. The electron energies are assumed to be so small that no excited states in the confined z-direction are possible (*i.e.* $n = 1$ in the equation (3.5)). Therefore the system is approximated to be two-dimensional.

In lateral quantum dots electrons are confined into the dot by the electric field of the external gate electrodes. This is modeled by using a parabolic potential

$$V_{\text{ext}}(\mathbf{r}) = \frac{1}{2} m^* \omega_0^2 r^2, \tag{7.1}$$

where $r^2 = x^2 + y^2$ and $\hbar\omega_0$ is the confinement strength. In the etched (vertical) quantum dots the confinement of the electrons is due to the edges of the dot. This is modeled using an infinite potential well potential, where

$$V_{\text{ext}}(x, y) = \begin{cases} 0, & \text{in the dot} \\ \infty, & \text{elsewhere.} \end{cases} \tag{7.2}$$

In this work the focus will be on the effects of geometry on the electronic structure of the quantum dots, the formation of the Wigner molecules in the weak confinement limit, and the effects of the magnetic field on quantum dot systems. An overview of the electronic structure calculations of SNS-junctions is also presented.

7.1 Effects of geometry in rectangular quantum dots

The electronic structure of square-shaped quantum dots has been previously studied theoretically by Bryant by using the configuration interaction method [50] and by Akbar

and Lee by using the spin-density-functional theory [51]. The theoretical considerations are in this work generalized to allow arbitrary rectangular form in paper IV. In experiments these have been realized by Austing *et. al* who applied electron-beam lithography with etching techniques on a double barrier heterostructure to form rectangular mesas of vertical quantum dots [52].

In the rectangular quantum dot the deformation parameter is defined as the ratio between the side lengths of the rectangle $\beta = L_x/L_y$. An infinite hard-wall potential is chosen to describe the external confinement of the electrons

$$V_{\text{ext}}(x,y) = \begin{cases} 0, & 0 \leq x \leq \beta L,\ 0 \leq y \leq L \\ \infty, & \text{elsewhere.} \end{cases} \tag{7.3}$$

The single electron states in a two-dimensional rectangular box can be written as

$$\psi_{n_x,n_y} = \frac{2}{L\sqrt{\beta}} \sin(\frac{n_x \pi x}{\beta L}) \sin(\frac{n_y \pi y}{L}), \tag{7.4}$$

where $n_x = 1, 2, 3, ...$ and $n_y = 1, 2, 3, ...$ are quantum numbers which label the eigenfunctions. The eigenenergies of these states are

$$E_{n_x,n_y} = \frac{\hbar^2 \pi^2}{2L^2} \left(\frac{n_x^2}{\beta^2} + n_y^2 \right). \tag{7.5}$$

In the non-interacting electron picture at zero temperature the lowest single electron states are occupied by one spin up and down electrons.

Calculations using the spin-density-functional theory (SDFT) have been performed in paper IV to determine the total energies of the rectangular quantum dots with different deformation parameters for up to 16 electrons. The results have also been obtained using the variational quantum Monte Carlo (VMC) method. The chemical potentials are calculated from the definition

$$\mu(N) = E(N) - E(N-1), \tag{7.6}$$

where $E(N)$ is the total energy for a system of N electrons. The addition energies are then defined as $\mu(N+1) - \mu(N)$ which in terms of the total energies can be written as $E(N-1) - 2E(N) + E(N+1)$.

For the square quantum dot ($\beta = 1$) the computational results are in good agreement with those by Akbar and Lee [51]. In that case the addition energies are higher for the 'magic numbers' $N = 2, 6, 8, 12, ...$ which correspond to closed shells (see figure 7.1 for explanation of the magic numbers). It turns out that the addition energies are very sensitive to the deformation parameter. *E.g.* the peak at $N = 8$ vanishes rapidly as the deformation parameter increases to $\beta = 1.2$. The results have been compared to experiments by Austing and coworkers [52]. The comparison is, however, difficult because of irregularities in the experimental dots and uncertainty in the deformation parameter. In spite of these problems similarities in the addition energy spectra can be found between the calculations and the experiments. The hard-wall potential (equation (7.3)) has been found to be a slightly better approximation than the elliptical potential described in the paper by Austing *et al.*.

The non-interacting electron picture determines the general electronic structure of rectangular quantum dots. The effect of electron-electron interactions has been studied using the SDFT and the VMC methods. The evolution of the ground-state spin S has been calculated as a function of the deformation parameter and the number of electrons. Partial polarizations have been found close to every degenerate point in the single electron spectrum which is in accord with Hund's rule. Spin-density-wave (SDW) -like solutions, which are mixtures of several paramagnetic states having $S = 0$ but different S_z, have been found close to the points where transition to spin-polarized $S = 1$ state takes place. The interpretation of these states is that breaking the internal spin symmetry lowers the total energy and keeps the quantum dot in the paramagnetic $S = 0$ state.

The SDFT was also used to study the quasi one-dimensional limit ($L_x \gg L_y$) which corresponds to a quantum-wire-like system. From the equation (7.5) one can see, that the second term of this expression, which corresponds to the energy of the the 2D-wave component in the squeezed direction, becomes very large in comparison to the component parallel to the long side of the rectangle. Therefore the lowest one-electron states in energy are the states $(n_x, 1)$. In the low density limit the system exists in a SDW-like state with N peaks. This corresponds to a Wigner molecule like electron density in which the electrons are localized on the 1D lattice sites [53]. In higher densities the spin densities start to overlap more and finally there is a transition to a spin symmetric charge-density wave (CDW) state with $N/2$ peaks. In this solution the electrons occupy delocalized one-electron states with one spin up and one spin down electron in each occupied state. The general behavior has been found out to be rather insensitive to the number of electrons in the system.

7.2 Wigner-molecule formation

The low density limit of the electron gas was considered by Wigner in 1934 [53]. He pointed out that if electrons had no kinetic energy, they would localize in configurations which correspond to the absolute minima of the potential energy. These configurations are close-packed lattice configurations of classical electrons known as Wigner crystals. In the electron gas the onset of a transition to a Wigner crystal happens already in finite kinetic energies and finite densities when the potential energy of the electron-electron interactions begins to dominate the kinetic energy. Quantum Monte Carlo simulations predict [54] that in the 3D electron gas the Wigner crystallization occurs in density for which $r_s = 100 \pm 20$, where the dimensionless parameter r_s is the radius of the sphere (or disc in 2D) which encloses one electron on the average.

For the 2D electron gas theory predicts a transition at $r_s = 1/(\sqrt{\pi n} a_B^*) \simeq 37$ [25]. In the experiments Wigner crystallization has been reported to happen in 2D electron gas at Si-MOSFETs accumulation layers [55]. The data in these experiments present evidence of a low temperature metal-insulator transition which is consistent with the picture of the 2D Wigner crystallization. The transition density corresponding to $r_s \simeq 10$, however, was much higher than the theory predicted. This discrepancy was attributed to disorder in the Si samples. Perturbation calculations and Monte Carlo simulations confirmed that impurity effects shift the transition in the 2D electron gas to densities which are consistent with the experiments [56].

Theoretical calculations show that electrons in quantum dots undergo a similar transition at low densities. By making the external potential sufficiently weak or the confining box large the electron-electron interactions finally localize the electrons. The resulting state is called a Wigner molecule. Various theoretical models have been used in the calculations, including exact diagonalization [57], quantum Monte Carlo [58], unrestricted Hartree-Fock [59] and spin-density-functional theory [60].

In this work the low density limit and the Wigner-molecule formation was studied in polygonal quantum dots by using the spin-density-functional theory (SDFT) in paper V. The model potentials are triangular, square, pentagonal and hexagonal in shape with hard-wall boundaries (equation (7.2)) The electron density is controlled by adjusting the size of the quantum dot.

Calculations have been performed first for the two-electron square dot and the results have been compared with the earlier work by Creffield and coworkers [57]. In the calculations the total Coulomb energy becomes increasingly more dominant over the kinetic energy as the size of the dot is enlarged. Following Creffield and coworkers, the criterion for the onset of Wigner-molecule formation in the case of the two-electron dot has been chosen to be the appearance of a minimum in the center of the dot. The transformation has been found to occur at $r_s \simeq 3$ and is independent of the chosen geometry. This is consistent with the calculations by Creffield and coworkers. Calculations with the SDFT in this work show appearances of spin-density-wave (SDW) -like ground states after the onset of the Wigner-molecule formation. In the case of triangles these appear at $r_s \simeq 3.5$ and for squares, pentagons and hexagons at $r_s \simeq 4.5$.

The Wigner-molecule formation has also been studied in larger systems up to 12 electrons in different geometries. The calculations have been performed to find out the electron density at the onset of the Wigner-molecule formation, and whether it depends on the electron density alone or if it depends on the chosen geometry and the number of electrons. In this case, the criterion of the Wigner-molecule formation is chosen as the appearance of as many density peaks as there are electrons in the system. The main result of these calculations is that the Wigner-molecule formation starts at $r_s \simeq 4.0$ and is largely independent of the chosen geometry and the number of electrons in the system. This figure can be compared to the Wigner crystallization of the 2D electron gas which, according to the simulations, occurs at $r_s \simeq 36$ (or $r_s \simeq 7.5$ in the presence of impurities). Higher transition density for the onset of Wigner-molecule formation can be attributed to the finite size of the system. This can be explained as follows: Assume an infinite close-packed Wigner lattice of electrons in 2D electron gas. Select a finite number of electrons by putting a hard-wall box (of insulating material) around the selected electrons. Imagine now that the negative charge of the surrounding electrons outside the box is removed. This causes the electrons inside the box to move closer to the hard-wall boundaries. The confinement also increases the kinetic energy of the electrons in the box, but calculations show, that the Coulomb energy dominates in this case. Therefore the localization of the electrons is increased and the onset of Wigner-molecule formation in a finite box happens at higher densities. When the number of selected electrons is very large the effect of surrounding electrons outside the box is negligible and the transition density to a Wigner molecule should shift close to the transition density in 2D electron gas. For systems consisting of up to 12 electrons we find, however, that the transition density is approximately constant.

7.3 Quantum dots in a magnetic field

The Schrödinger equation for a single electron moving in a 2D harmonic potential and uniform magnetic field is

$$\left(\frac{1}{2m^*}\left[-i\hbar\nabla + e\mathbf{A}(\mathbf{r})\right]^2 + \frac{1}{2}m^*\omega_0^2 r^2\right)\psi = E\psi. \tag{7.7}$$

This equation can be analytically solved [61]. The resulting states are known as the Fock-Darwin states which can be expressed using two quantum numbers $n = 0, 1, 2, ...$ and $l = 0, \pm 1, \pm 2, ...$, *i.e.* the principal quantum number and the angular momentum quantum number, respectively. Using $\omega_c = eB/m^*$ to denote the cyclotron frequency of the electron the energy eigenvalues are

$$E_{n,l} = (2n + |l| + 1)\hbar\omega - \frac{\omega_c\hbar l}{2}, \tag{7.8}$$

where $\omega = \sqrt{\omega_0^2 + (\omega_c/2)^2}$. The energy levels bunch in high magnetic fields to form the Landau-levels (see figure 7.1). This exact solution is of limited use in the electronic structure calculations of the quantum dots because it applies only to the single-electron quantum dot with parabolic confinement. However, the Fock-Darwin states are useful in the classification of the one-electron states of the density-functional calculations.

In the interacting many-electron case, the Schrödinger equation cannot be solved exactly. One of the widely used tools in the electronic structure calculations of the few-electron systems is exact diagonalization [62]. The exact solution of the Schrödinger equation is a state vector in a Hilbert space which has an infinite set of basis vectors. In the exact diagonalization technique, only a finite set of basis vectors is used and the solution is calculated in this subspace. The eigenenergies obtained in this subspace obey the variational principle. Contrary to its name, exact diagonalization does not provide an exact solution to the many-body problem but a solution that can be made arbitrarily accurate by making the subspace larger. Unfortunately, exact diagonalization becomes computationally heavy as the number of particles in the system increases. With present day computers this method is limited to systems consisting of at most 5 electrons.

In the present work the electronic structure calculations have been performed for a six-electron quantum dot in parabolic confinement with the spin-density-functional theory (SDFT) and current-spin-density-functional theory (CSDFT). The results are compared to variational quantum Monte Carlo results for magnetic field up to 11 T. The qualitative results[1] for the six-electron quantum dot in high magnetic fields are shown in figures 7.2 and 7.3. The figure 7.2 shows the evolution of the electron density and the figure 7.3 shows the physical current density at 18 T. Similar vortices were found by Reimann and coworkers in the CSDFT calculations using the plane-wave approach [63]. There is a formation of a symmetric flat electron density with sharp edges at about 4.8 T. This is known as the maximum density droplet (MDD) and is totally spin polarized, with the z component of the total spin $S_z = 3$. The one-electron states $n = 0$, $l = 0, 1, 2, ..., 5$ are occupied in the MDD state giving the z-component of the total angular momentum $L_z = 15$. After the MDD state at about 10 T there is a charge density wave (CDW)

[1] These results are unpublished.

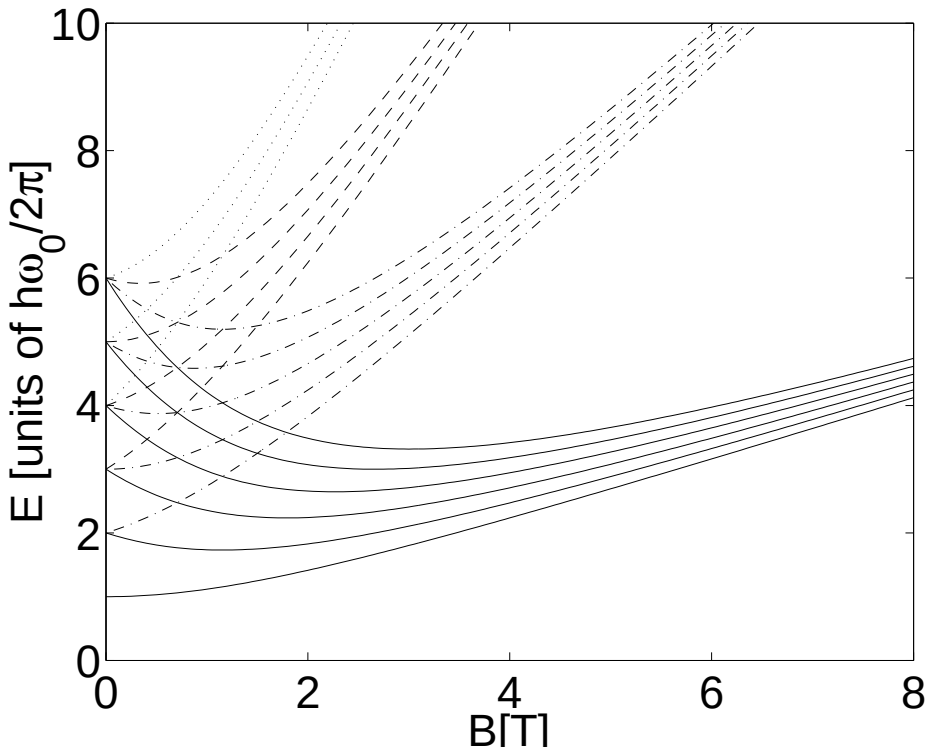

Figure 7.1: Fock-Darwin states for a single electron moving in a 2D harmonic potential and a uniform magnetic field perpendicular to the plane. Only the first 18 levels which are the lowest lying levels at $B = 0$ are shown. The energy levels bunch in high magnetic fields to form the lowest Landau-level (solid line) for the $n = 0,\ m = 0, 1, 2, ...$, the second Landau-level (dash-dotted line) for the $n = 0,\ m = -1$ and $n = 1,\ m = 0, 1, 2, ...$ and the higher Landau-levels (dashed and dotted lines). The figure also explains the magic numbers in the addition energy spectrum of the 2D quantum dots. In zero magnetic field the lowest one-electron state has the degeneracy of 1. The second lowest state is $\hbar\omega_0$ higher in energy and has the degeneracy of 2 and so on. If we assume that each state can occupy one-spin up and one spin-down electron, we get closed shells at the electron numbers $2, 6, 12, 20, ...$ This can be compared to the magic numbers for electrons in 3D harmonic potential $2, 10, 18, ...$, which are the atomic numbers of noble gas atoms.

solution with six peaks which breaks the rotational symmetry. Numerically calculated L_z for the CDW solution gets a fractional value and increases as the magnetic field is increased. In very high magnetic fields vortices start to form in the quantum dot. There is a jump in the L_z when the number of vortices increases. The L_z is increased to about 40 at 20 T. Calculations show that the vortex structure is sensitive to variations in the strength of the confining potential.

A double dot 'hydrogen molecule' system in a magnetic field has been studied in paper I. The inter-dot distance has been chosen to be 2.73 a_B^* and the confinement strength of the two dots are $\hbar\omega_0 = 3$ meV. The ground states of the double dot with the total spin S=0 (singlet) and S=1 (triplet) provide a possible realization for a cubit of the quantum computer [64]. The model potential has been chosen to be a quartic potential

$$V_{\text{ext}}(x,y) = \frac{m^*\omega_0^2}{2}\left[\frac{1}{4a^2}(x^2-a^2)^2 + y^2\right], \tag{7.9}$$

where the centres of the dots are at $x = \pm a$. The inter-dot distance $d = 2a$. The singlet-triplet energy separation has been calculated with the CSDFT as a function of magnetic field up to 6 T. The exchange-correlation energy e_{xc} has been chosen to be the Padé approximant (5.21) and the Tanatar-Ceperley functionals (5.8) are used for the zero-field limits of e_{xc}. The evolution of the electron density is shown in the figure 7.4 and the singlet-triplet separation is shown in the figure 7.5. The first transition from triplet state to singlet state has been found to be at about 1.4 T. A similar system has been considered by A. Harju and coworkers by using direct diagonalization of the Hamiltonian. They found the first transition at 1.25 T which agrees quite well with the CSDFT calculations. The Hund-Mulliken and Heitler-London approximations give transition magnetic field which are in qualitative agreement with the CSDFT results [64].

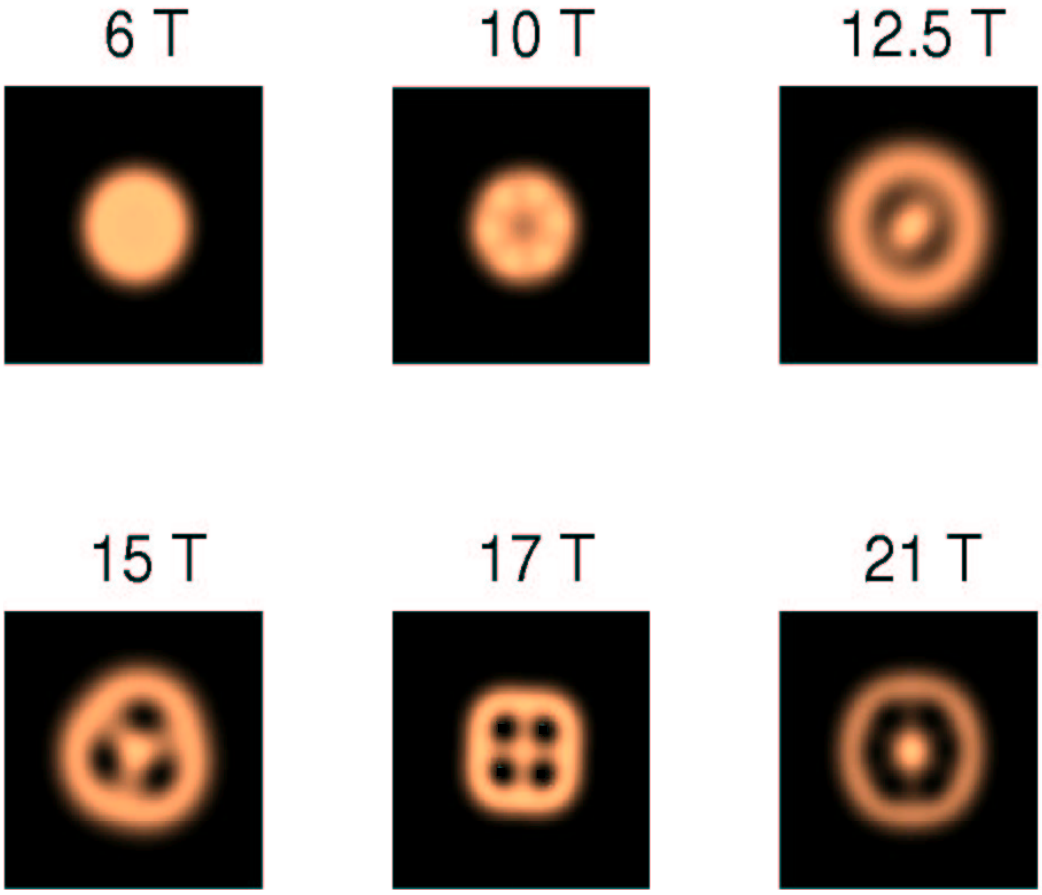

Figure 7.2: Electron density of a six-electron quantum dot in high magnetic fields. The confinement is parabolic with $\hbar\omega_0 = 5\,\mathrm{meV}$. The flat electron density is a characteristic of the maximum density droplet (MDD) solution at 6 T. At 10 T a charge-density-wave (CDW) solution appears. In high magnetic fields vortices start to form in the dot. The physical current density in the case of 4-vortex solution is shown in the figure 7.3.

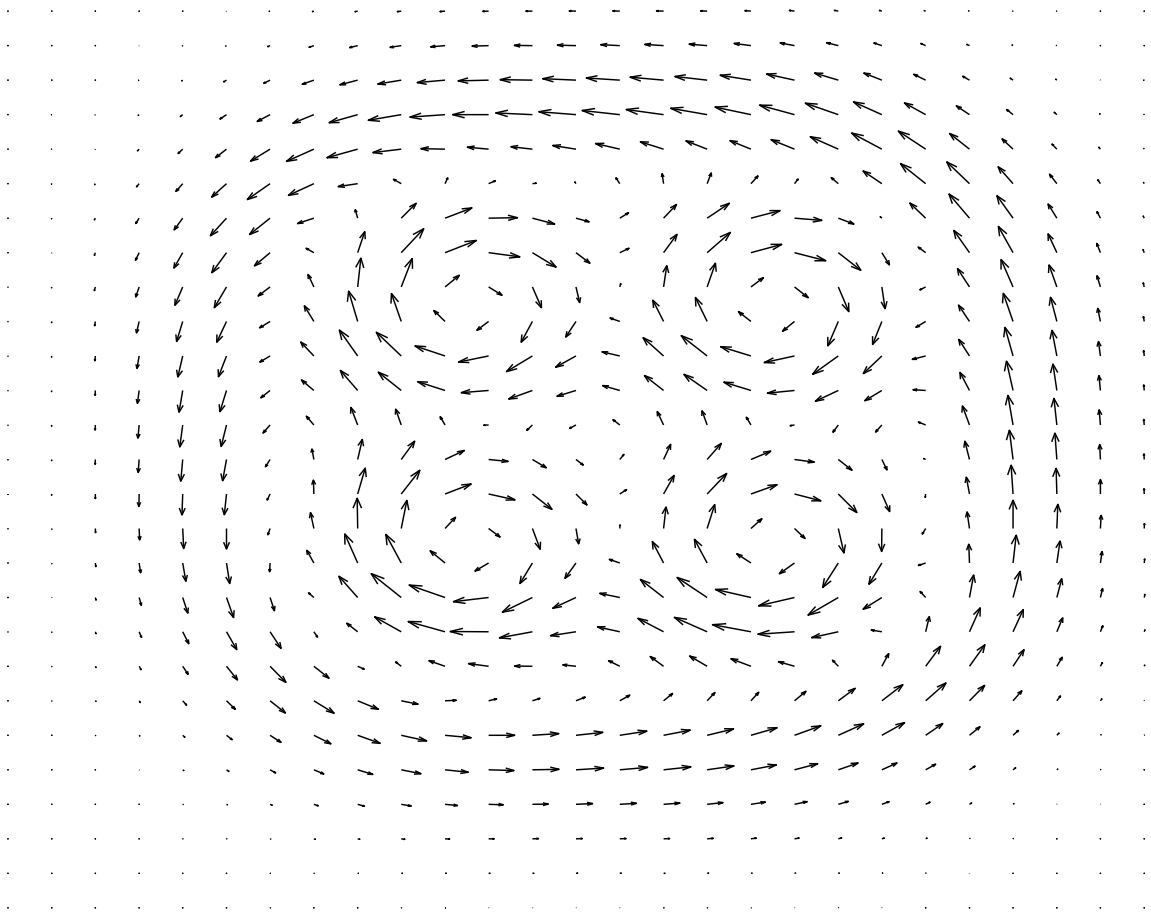

Figure 7.3: Physical current density in a 6-electron dot at 18 T. The confinement is parabolic with $\hbar\omega_0 = 5\,\mathrm{meV}$. The picture shows four vortices around which the current is circulating.

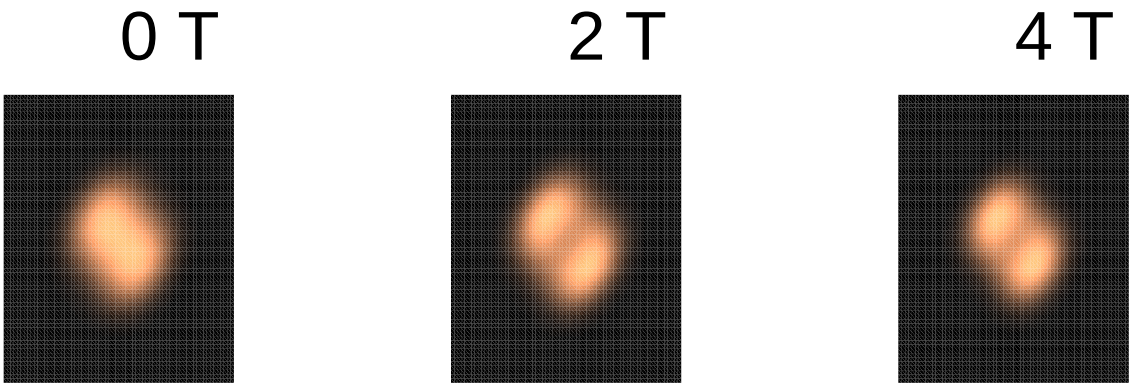

Figure 7.4: Evolution of the electron density of the double dot system. The inter-dot distance is 2.73 a_B^* and the confinement strengths of the dots are $\hbar\omega_0 = 3$ meV. At 0 T the ground state is the singlet state. There is a transition to triplet state at $B \simeq 1.4$ T. The electron density of the triplet state is more localized to the dot centres.

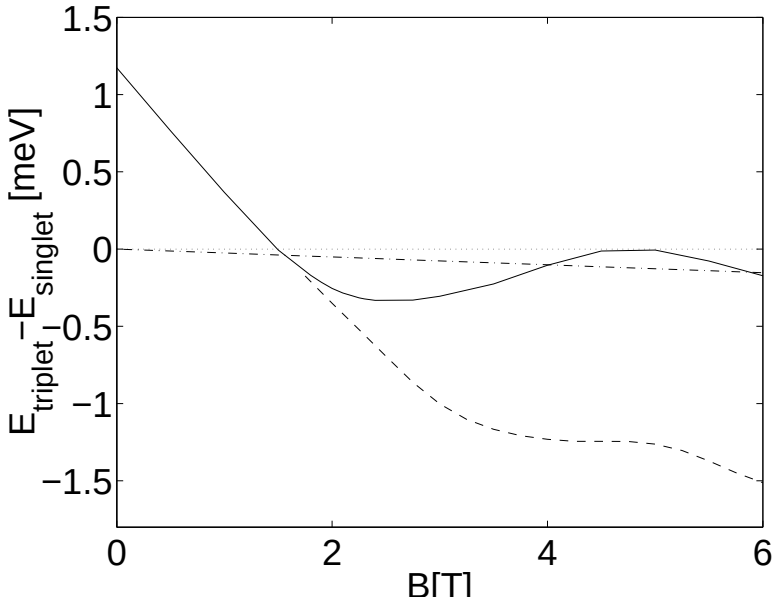

Figure 7.5: Two-electron double dot. The inter-dot distance is 2.73 a_B^* and the confinement strengths of the dots are $\hbar\omega_0 = 3$ meV. The singlet-triplet energy separation (solid line) is given as a function of the external magnetic field B. The calculations were performed using the CSDFT within the LSDA. The results corresponding to the symmetry-preserving, spin-compensated CSDFT-LDA are also shown (dashed line). The magnitude of the Zeeman term is also plotted (dash-dotted line).

7.4 SNS junction

The combination of quantum dots with superconducting materials creates an interesting system both for basic research and for potential applications. Josephson predicted in 1962 that a supercurrent can persist in a superconducting lead if a thin insulator is put between the leads to form a superconductor-insulator-superconductor (SIS) structure [65]. The theoretical explanation is that due to the large coherence length of the superconductors the Cooper pairs forming the supercurrent can tunnel across the junction. Since in certain SIS junctions the superconducting current is highly sensitive to a magnetic field this phenomenon allows construction of fast electronic switches known as superconducting quantum interference devices (SQUIDs). In general superconductors can also be combined with a mesoscopic weak link to form superconductor-normal metal-superconductor (SNS) structures. This creates a field of potential applications, *e.g.* Josephson field effect transistors (JOFETS) and injected-current SNS transistor.

In the superconductor-normal quantum dot-superconductor structure the gate electrode attracts and confines electronic charge to the quantum dot. The Cooper pairs of the supercurrent are then transported through the normal region in the process which is called Andreev reflection [66, 67]. In the Andreev reflection an electron-like quasi-particle converts to a hole-like quasi-particle in the normal quantum dot-superconductor interface which then reflects back to the dot and a Cooper pair is transmitted into the superconductor. This process creates states in the normal quantum dot which are called Andreev bound states. These states carry most of the current through the structure in a short junction [68].

The effect of electron-electron interactions on the supercurrent has been investigated analytically and computationally in papers VI and VII. The numerical analysis is done using two-component density-functional theory (DFT). In paper VI this is done in 1D and the method is generalized to 2D in paper VII. The Andreev state charge is solved using the Bogoliubov-de Gennes equation

$$\begin{pmatrix} H(x) & \Delta(x) \\ \Delta^*(x) & -H(x) \end{pmatrix} \begin{pmatrix} u_\kappa(x) \\ v_\kappa(x) \end{pmatrix} = \epsilon_\kappa \begin{pmatrix} u_\kappa(x) \\ v_\kappa(x) \end{pmatrix}, \tag{7.10}$$

where u_κ and v_κ are the two components of the wave function $\Psi(x) = (u(x), v(x))$, H is the effective Hamiltonian, ϵ_κ is the energy eigenvalue, and Δ is the pair potential. The equation (7.10) is discretized and the problem reduces to a generalized eigenvalue problem $K(\epsilon)\Psi = \epsilon\Psi$, where K is a matrix operator and $\Psi = (u, v)$ is the state vector. Since the $K(\epsilon)$ matrix depends on the eigenvalue ϵ an iterative Arnoldi method has been applied for the solution of the generalized eigenvalue problem. The localized states in the normal quantum dot are solved using a multigrid method for the 1D Schrödinger equation in the 1D formulation of the problem. A self-consistent density-functional formalism is used in the 2D formulation.

The main result of these calculations is that the supercurrent is enhanced in the presence of Coulomb interactions in the normal quantum dot compared to the noninteracting electron approximation. Thus, the supercurrent can be controlled by the gate voltage of the quantum dot.

Chapter 8

SUMMARY

The main objectives of this work have been the electronic structure calculations of quantum dots. Emphasis has also been set on developing and testing the various methods and approximations which are useful in these calculations. The methods have been applied to the study of quantum dot systems in zero and finite magnetic fields.

The spin-density-functional theory (SDFT) and the current-spin-density-functional theory (CSDFT) have been used in the electronic structure calculations in real space. These theories have been used in combination with local approximations for the exchange-correlation energy. In papers I–III the reliabilities of these methods have been studied by comparing the results with the quantum Monte Carlo calculations. The model system in the tests has been a six-electron quantum dot with a parabolic confinement. The confinement strength has been chosen to be $\hbar\omega_0 = 5$ meV. The results of these tests indicate that the CSDFT gives a better approximation for the ground-state energy than the SDFT for the spin-polarized maximum-density-droplet (MDD) solution and for states beyond this MDD state. The transition to the MDD state occurred in the model system at $B \simeq 5$T.

The ground-state energy and the electronic structure turn out to be sensitive to the choice of the exchange-correlation energy functional, especially in the CSDFT. The exact form of this potential is not known and several functionals have been proposed. They give accurate results for the totally spin-polarized states but the accuracy is worse for the partially polarized states. The result of the present work calls for further Monte Carlo simulations for partially polarized 2D electron gas in an external magnetic field. Moreover, Monte Carlo simulation data is needed for a satisfactory interpolation formula between the high and low vorticity limits of the exchange-correlation energy.

The ground-state electronic structures of quantum dot systems in external magnetic fields have been studied in papers I–III. Symmetry-breaking solutions emerge in high magnetic fields. These include spin-density-wave-like solutions, charge-density-wave-like solutions, and solutions with vortex structures. The structure and properties of these solutions have been calculated and the interpretation of the broken symmetry discussed.

The ground-state properties of quantum dots have also been studied in zero magnetic field. The Wigner-molecule formation has been studied in paper V. The effects of the

shape of the dot and the number of electrons in the system have been studied. The results are rather insensitive to both parameters. An approximate criterion for the onset of the Wigner-molecule formation has been calculated, and can be compared to results from experiments. In paper IV calculations have been done for the ground-state of rectangular quantum dots. This paper includes also a tentative comparison with the experiments by Austing and coworkers. The results suggest that the rectangular model potential gives a somewhat better fit to the experimental data compared to the elliptical model potential.

Finally, this work includes a theoretical study of a superconductor-normal quantum dot-superconductor (SNS) junction in papers VI and VII. In these papers numerical solution techniques for Andreev states are combined with the numerical solution techniques developed and tested in the preparation of this thesis. Calculations are then performed to investigate the effect of electron-electron interactions in the dot on the supercurrent through the SNS junction. The results indicate that these interactions enhance the supercurrent and therefore the supercurrent can be controlled by using the gate electrode of the quantum dot.

Appendix A

Abstracts of the publications I–VII

I H. Saarikoski, E. Räsänen, S. Siljamäki, A. Harju, M. J. Puska, and R. M. Nieminen, *Electronic properties of model quantum-dot structures in zero and finite magnetic fields*, European Journal of Physics B, **26**, 241–252 (2002). In this paper ground-state electronic structures of quantum dots and a quantum dot molecule in external magnetic field are studied using the spin-density-functional theory and the current-spin-density-functional theory. The methods are applied using a symmetry-unrestricted real space approach. Reliability of the results is discussed by comparing the results with those obtained with the variational quantum Monte Carlo method. The structure and role of the symmetry-breaking solutions are discussed.

II H. Saarikoski, M. J. Puska, and R. M. Nieminen, *Electronic structure calculations for two-dimensional quantum dots and laterally coupled quantum-dot molecules in magnetic fields*, International Journal of Quantum Chemistry **91** (3): 490–497 (2003). This paper is a conference paper of the DFT2001 conference. Quantum dot systems are studied using the spin-density-functional theory and the current-spin-density-functional theory. The paper concentrates on the electronic structure of a six-electron quantum dot and a double dot 'hydrogen' molecule. The computational method is presented with details.

III H. Saarikoski, E. Räsänen, S. Siljamäki, A. Harju, M. J. Puska, and R. M. Nieminen, *Testing of two-dimensional local approximations in the current-spin and spin-density-functional theories*, Physical Review B **67**, 205 327 (2003). This paper deals with the problem of choosing an accurate exchange-correlation potential. A model quantum dot system in an external magnetic field is studied by using both the spin-density-functional theory and the current-spin-density-functional theory. The theories are used with local approximations for the spin-density and the vorticity. The reliabilities of different parametrizations for the exchange-correlation functionals are tested by comparing the ensuing energetics with quantum Monte Carlo results. The limit where the vorticity dependence should be used in the exchange-correlation functionals is discussed. New LSDA functional by Attaccalite *et al.* gives in the zero magnetic field much better results for the total energy than the old form by Tanatar and Ceperley. The tests indicate that

exchange-correlation potentials in CSDFT are accurate for the zero field case and for spin-polarized systems, but the accuracy is worse for the partially spin-polarized systems due to lack of relevant Monte Carlo simulation data for 2D electron gas.

IV E. Räsänen, H. Saarikoski, V.N. Stavrou, A. Harju, M. J. Puska, and R. M. Nieminen, *Electronic structure of rectangular quantum dots*, Physical Review B, **67**, 235 307 (2003). Ground-state properties of rectangular quantum dots are studied using the spin-density-functional theory and the variational quantum Monte Carlo method. The results indicate that the electronic structure is very sensitive to deformation. Spin-density-wave and charge-density-wave states are found as well as strongly localized states. Tentative common features with the experiments are found in the addition energy spectra. The results suggest that the rectangular model potential gives a somewhat better fit to the experimental data compared to the elliptical model potential.

V E. Räsänen, H. Saarikoski, M. J. Puska, and R. M. Nieminen, *Wigner molecules in polygonal quantum dots: A density-functional study*, Physical Review B, **67**, 035 326 (2003). Spin-density-functional theory is applied in studying the electronic structure of the polygonal (triangle, square, pentagonal and hexagonal) quantum dots in zero magnetic field. Transition to the Wigner molecule state is studied and compared to the results of the exact diagonalization. We find out that the density in which the transition to a Wigner molecule occurs is rather insensitive to both the shape of the dot and the number of electrons. From the calculations we obtain an approximate criterion $r_s \simeq 4.0$ for the onset of Wigner-molecule formation.

VI Klas Engström, Jari Kinaret, Robert I. Shekhter, Martti Puska, and Henri Saarikoski, *Influence of electron-electron interactions on current through SNS structures*, Low Temperature Physics (Fizika Nizkikh Temperatur), **29**, 546 (2003). Superconductor-normal quantum dot-superconductor (SNS) structure is considered. The effect of the electron-electron interactions on the supercurrent is studied. The SNS junction is modeled using the Bogoliubov-de Gennes-Kohn-Sham equations in one-dimensional space. The localized normal states in the quantum dot are solved using the multigrid method. It is shown that the gate voltage in the quantum dot can be used to control the supercurrent.

VII Klas Engström, Jari Kinaret, Robert I. Shekhter, Henri Saarikoski, and Martti Puska, *Interaction effects in superconductor-normal quantum dot-superconductor structures*, Submitted to Computational Materials Science. Superconductor-normal quantum dot-superconductor (SNS) structure is analyzed using a two-dimensional model for the junction. The electron density of the confined charge in the quantum dot is solved using the density-functional theory. Results indicate that interactions in the normal quantum dot increase the supercurrent through the structure.

Bibliography

[1] P. McEuen. Science **278**, 1729 (1997).

[2] L. P. Kouwenhoven, D. G. Austing, and S. Tarucha. Rep. Prog. Phys. **64**, 701 (2001).

[3] L. Jacak, P. Hawrylak, and A. Wójs. *Quantum Dots* (Springer-Verlag, 1998).

[4] G. van der Wiel, S. D. Franceschi, J. M. Elzerman, T. Fujisawa, S. Tarucha, and L. P. Kouwenhoven. Rev. Mod. Phys. **75**, 1 (2003).

[5] H. Ibach and H. Lüth. *Solid-State Physics* (Springer-Verlag, 1995), 2nd edition.

[6] A. O. Orlov, I. Amlani, G. H. Bernstein, C. S. Lent, and G. L. Snider. Science **277**, 928 (1997).

[7] D. Loss and D. P. DiVincenzo. Phys. Rev. A **57**, 120 (1998).

[8] M. Jammer. *The Conceptual Development of Quantum Mechanics* (McGraw-Hill, 1966).

[9] S. Gasiorowicz. *Quantum Physics* (Wiley, 1974), 2nd edition.

[10] P. G. de Gennes. *Superconductivity of Metals and Alloys* (Perseus Books, 1966).

[11] P. W. Anderson. Science **177**, 393 (1972).

[12] M. Tinkham. *Group theory and Quantum mechanics* (McGraw-Hill, 1964).

[13] S. Elliott. *The Physics and Chemistry of Solids* (Wiley, 1998).

[14] M. Born and R. Oppenheimer. Ann. Phys. (Leipzig) **84**, 457 (1927).

[15] S. Datta. *Electronic Transport in Mesoscopic Systems* (Cambridge University Press, Cambridge, 1995).

[16] S. E. Koonin. *Computational Physics* (Benjamin/Cummings, Menlo Park, 1986).

[17] H. Gould and J. Tobochnik. *An Introduction to Computer Simulation Methods* (Addison-Wesley, 1996), 2nd edition.

[18] P. Hohenberg and W.Kohn. Phys. Rev. **136**, B846 (1964).

[19] W. Kohn and L. Sham. Phys. Rev. **140**, A1133 (1965).

[20] A. Göring. Phys. Rev. A **59**, 3359 (1999).

[21] O. Gunnarsson and B. I. Lundqvist. Phys. Rev. B **13**, 4274 (1976).

[22] U. von Barth. Phys. Rev. A **20**, 1693 (1979).

[23] H. Eschrig and W. E. Pickett. Solid State Commun. **118**, 123 (2001).

[24] K. Capelle and G. Vignale. Phys. Rev. B **86**, 5546 (2001).

[25] B. Tanatar and D. M. Ceperley. Phys. Rev. B **39**, 5005 (1989).

[26] M. Koskinen, M. Manninen, and S. M. Reimann. Phys. Rev. Lett. **79**, 1389 (1997).

[27] C. Attaccalite, S. Moroni, P. Gori-Giorgi, and G. B. Bachelet. Phys. Rev. Lett. **88**, 256601 (2002).

[28] P. Gori-Giorgi, C. Attaccalite, S. Moroni, and G. B. Bachelet. Int. J. Quantum Chemistry **91**, 126 (2003).

[29] J. P. Perdew and Y. Wang. Phys. Rev. B **45**, 13 244 (1992).

[30] G. Vignale and M. Rasolt. Phys. Rev. B **37**, 10 685 (1988).

[31] D. Levesque, J. J. Weis, and A. H. MacDonald. Phys. Rev. B **30**, 1056 (1984).

[32] G. Fano and F. Ortolani. Phys. Rev. B **37**, 8179 (1988).

[33] R. Price and S. D. Sarma. Phys. Rev. B **54**, 8033 (1996).

[34] M. Rasolt and F. Perrot. Phys. Rev. Lett. **69**, 2563 (1992).

[35] O. Heinonen, M. I. Lubin, and M. D. Johnson. Phys. Rev. Lett. **75**, 4110 (1995).

[36] M. Koskinen, J. Kolehmainen, S. M. Reimann, J. Toivanen, and M. Manninen. Eur. Phys. J. D **9**, 487 (1999).

[37] M. Ferconi and G. Vignale. Phys. Rev. B **50**, 14 722 (1994).

[38] H. A. Jahn and E. Teller. Proc. R. Soc. London, Ser. A **161**, 220 (1937).

[39] S. M. Reimann and M. Manninen. Rev. Mod. Phys. **74**, 1283 (2002).

[40] K. Hirose and N. S. Wingreen. Phys. Rev. B **59**, 4604 (1999).

[41] T. L. Beck. Rev. Mod. Phys. **72**, 1041 (2000).

[42] W. H. Press, B. P. Flannery, S. A. Teukolsky, and W. T. Vetterling. *Numerical recipes in FORTRAN* (Cambridge University Press, Cambridge, England, 1992).

[43] P. Maragakis, J. Soler, and E. Kaxiras. Phys. Rev. B **64**, 193101 (2001).

[44] C.-K. Skylaris, O. Diéguez, P. D. Haynes, and M. C. Payne. Phys. Rev. B **66**, 073103 (2002).

[45] W. L. Briggs, V. E. Henson, and S. F. McCormick. *A Multigrid Tutorial* (Society for Industrial and Applied Mathematics, 2000), 2nd edition.

[46] M. Heiskanen, T. Torsti, M. J. Puska, and R. M. Nieminen. Phys. Rev. B **63**, 245106 (2001).

[47] J. Mandel and S. McCormick. J. Comput. Phys. **80**, 442 (1989).

[48] J. Vanderlinde. *Classical Electromagnetic Theory* (Wiley, 1993).

[49] C. Weisbuch and C. Hermann. Phys. Rev. B **15**, 816 (1977).

[50] G. W. Bryant. Phys. Rev. Lett. **59**, 1140 (1987).

[51] S. Akbar and I.-H. Lee. Phys. Rev. B **63**, 165 301 (2001).

[52] D. Austing, S. Sasaki, S. Tarucha, S. M. Reimann, M. Koskinen, and M. Manninen. Phys. Rev. B **60**, 11 514 (1999).

[53] E. P. Wigner. Phys. Rev. **46**, 1002 (1934).

[54] D. M. Ceperley and B. J. Alder. Phys. Rev. Lett. **45**, 566 (1980).

[55] V. M. Pudalov, M. D'Iorio, S. V. Kravchenko, and J. W. Campbell. Phys. Rev. Lett. **70**, 1866 (1993).

[56] S. T. Chui and B. Tanatar. Phys. Rev. Lett. **74**, 458 (1995).

[57] C. E. Creffield, W. Häusler, J. H. Jefferson, and S. Sarkar. Phys. Rev. B **59**, 10 719 (1999).

[58] A. Harju, S. Siljamäki, and R. M. Nieminen. Phys. Rev. B **65**, 075 309 (2002).

[59] B. Reusch, W. Häusler, and H. Grabert. Phys. Rev. B **63**, 113313 (2001).

[60] S. M. Reimann, M. Koskinen, and M. Manninen. Phys. Rev. B **62**, 8108 (2000).

[61] V. Fock. Z. Phys. **47**, 446 (1928).

[62] S. Raimes. *Many-Electron theory* (North-Holland Publishing Comp., Amsterdam, London, 1972).

[63] S. M. Reimann, M. Koskinen, M. Manninen, and B. R. Mottelson. Phys. Rev. Lett. **83**, 3270 (1999).

[64] G. Burkard, D. Loss, and D. P. DiVincenzo. Phys. Rev. B **59**, 2070 (1999).

[65] B. D. Josephson. Phys. Lett. **1**, 251 (1962).

[66] A. F. Andreev. Sov. Phys. JETP **19**, 1228 (1964).

[67] A. F. Andreev. Sov. Phys. JETP **22**, 455 (1966).

[68] C. W. J. Beenakker and H. van Houten. Phys. Rev. B **26**, 241 (1991).